blood RCI
red cells & iron

American Society of Hematology
2021 L Street NW, Suite 900,
Washington, DC 20036
Phone: 202-776-0544 | Fax 202-776-0545
bloodrci@hematology.org

Disease-modifying effects of iron deficiency in mouse models of chronic renal failure

Tracking no: RCI-2025-000104R1

Moya Zhang (David Geffen School of Medicine at UCLA, United States) Amber Lundin (David Geffen School of Medicine at UCLA, United States) Grace Jung (UCLA, United States) Joseph Olivera (David Geffen School of Medicine at UCLA, United States) Veena Sangkhae (David Geffen School of Medicine at UCLA, United States) Shilpa Sharma (David Geffen School of Medicine at UCLA, United States) Tomas Ganz (David Geffen School of Medicine at UCLA, United States) Elizabeta Nemeth (David Geffen School of Medicine at UCLA, United States) Mark Hanudel (UCLA, United States) Brian Czaya (David Geffen School of Medicine at UCLA, United States)

Abstract:
Chronic kidney disease (CKD) impacts global health, contributing to one in sixty fatalities worldwide. Iron deficiency (ID), a common complication of CKD, is a major cause of years lived with disability. The combination of CKD and ID presents a particularly challenging health burden, as ID can exacerbate CKD-related complications and negatively impact patient outcomes. Despite the high prevalence of ID and anemia in patients with CKD, whether and how ID alters CKD-associated complications such as systemic inflammation, organ fibrosis, vascular calcification, and cardiomyopathy remains insufficiently understood. Employing two distinct mouse models of CKD, adenine-induced nephropathy and Alport syndrome (Col4a3-/-), we induced moderate or severe ID in mice and investigated how it modulates pathological complications. At baseline, akin to patients with CKD, both adenine nephropathy and Alport models displayed systemic inflammation, vascular calcification, and kidney and cardiac injury accompanied by fibrosis. Severe ID aggravated systemic inflammation, kidney fibrosis, and cardiac fibrosis in adenine-induced CKD, while showing no significant effect on vascular calcification, kidney injury, kidney functional impairment, or pathologic cardiac remodeling in either model. Our study offers valuable insights into the pathophysiologic mechanisms driving CKD-related comorbidities, and suggests that iron supplementation may be beneficial in mitigating specific aspects of inflammation-induced kidney damage.

Conflict of interest: COI declared - see note

COI notes: The authors declare competing financial interests: TG and EN are shareholders and scientific advisers of Intrinsic LifeSciences and Silarus Therapeutics, and consultants for Disc Medicine, Ionis Pharmaceuticals, Protagonist, Vifor, GSK, Chiesi, Novo Nordisk (EN), Silence Therapeutics, Intrinsic LifeSciences. Ionis Pharmaceuticals, Disc Medicine, City Therapeutics, Chugai, Dexcel, BristolMyersSquib 65. Other authors report no conflict of interest.

Preprint server: No;

Author contributions and disclosures: MZ performed experiments and analyzed data. AL, GJ, JO, VS assisted with experiments. SS, TG, EN, MH helped conceive and plan the project, and assisted with data interpretation and manuscript editing. BC conceived the project, designed and performed experiments, analyzed data, prepared figures, and wrote the manuscript. All authors discussed results, read and contributed edits to manuscript, and approved final version.

Non-author contributions and disclosures: No;

Agreement to Share Publication-Related Data and Data Sharing Statement: For original data, please contact BCzaya@mednet.ucla.edu

Clinical trial registration information (if any):

Title page

Disease-modifying effects of iron deficiency in mouse models of chronic renal failure

Authors and Affiliations:

Moya Zhang[1#], Amber Lundin[1#], Grace Jung[1], Joseph D. Olivera[1], Veena Sangkhae[1], Shilpa Sharma[1,2], Tomas Ganz[1], Elizabeta Nemeth[1], Mark R. Hanudel[1,3] and Brian Czaya[1*]

[1]Center for Iron Disorders, Department of Medicine, David Geffen School of Medicine at UCLA, Los Angeles, California, USA

[2]Division of Nephrology, David Geffen School of Medicine at UCLA, Greater Los Angeles Veterans Affairs Healthcare System, Los Angeles, California USA

[3]Department of Pediatrics, David Geffen School of Medicine at UCLA, Los Angeles, CA, USA

[#]These authors contributed equally

***Lead Contact Information:**

Brian Czaya, Ph.D

43-229 CHS; 10833 LeConte Ave

Los Angeles, CA, 90095, USA

Telephone: 310-825-7499; Fax: N/A; Email: BCzaya@mednet.ucla.edu

Running headline

Iron deficiency potentiates systemic complications in adenine-CKD

Data Sharing Statement: For original data, please contact BCzaya@mednet.ucla.edu

Abstract word count: 201

Text word count: 4,399

Number of Figures: 6

Number of Tables: 0

Number of References: 71

Key Points

- Iron deficiency, particularly when severe, intensifies systemic inflammation, kidney fibrosis, and cardiac fibrosis in CKD

Abstract

Chronic kidney disease (CKD) impacts global health, contributing to one in sixty fatalities worldwide. Iron deficiency (ID), a common complication of CKD, is a major cause of years lived with disability. The combination of CKD and ID presents a particularly challenging health burden, as ID can exacerbate CKD-related complications and negatively impact patient outcomes. Despite the high prevalence of ID and anemia in patients with CKD, whether and how ID alters CKD-associated complications such as systemic inflammation, organ fibrosis, vascular calcification, and cardiomyopathy remains insufficiently understood. Employing two distinct mouse models of CKD, adenine-induced nephropathy and Alport syndrome (*Col4a3*$^{-/-}$), we induced moderate or severe ID in mice and investigated how it modulates pathological complications. At baseline, akin to patients with CKD, both adenine nephropathy and Alport models displayed systemic inflammation, vascular calcification, and kidney and cardiac injury accompanied by fibrosis. Severe ID aggravated systemic inflammation, kidney fibrosis, and cardiac fibrosis in adenine-induced CKD, while showing no significant effect on vascular calcification, kidney injury, kidney functional impairment, or pathologic cardiac remodeling in either model. Our study offers valuable insights into the pathophysiologic mechanisms driving CKD-related comorbidities, and suggests that iron supplementation may be beneficial in mitigating specific aspects of inflammation-induced kidney damage.

Introduction

Chronic kidney disease (CKD) is a global health challenge affecting over 800 million individuals in both developed and developing nations.[1,2] With no effective treatments to cure this disease, clinical management prioritizes the mitigation of factors that contribute to CKD progression.[3,4] CKD is often exacerbated by systemic complications such as anemia, inflammation, organ fibrosis and vascular calcification.[5-9] These conditions drive cardiovascular disease, the leading cause of premature death in CKD.[10]

A prominent aspect of CKD is altered iron homeostasis, with a high prevalence of iron deficiency (ID) and anemia.[11-13] Anemia in CKD is associated with poor outcomes including cognitive impairment, and mortality.[14,15] The etiology of this anemia is driven by a complex interplay of reduced red blood cell lifespan, relative erythropoietin deficiency, systemic inflammation, and both absolute and functional ID.[16] Absolute ID occurs when total body iron stores are depleted, whereas functional ID arises when iron stores are adequate but insufficiently mobilized to support erythropoiesis.[17] This iron restriction is driven by elevated hepcidin levels, which are increased by inflammatory cytokines, mainly interleukin-6.[18,19] Hepcidin is a key regulator of iron homeostasis, controlling flow of iron into circulation by inhibiting ferroportin, the sole known cellular iron exporter.[20] This inhibition restricts iron efflux from iron recycling macrophages and duodenal enterocytes, leading to reduced serum iron levels (hypoferremia) and erythropoiesis. Chronically inadequate intestinal iron absorption combined with increased blood loss contributes to development of absolute ID.[21,22]

Anemia worsens quality of life and outcomes in CKD.[16,23-25] Notably, ID and anemia might accelerate kidney injury progression, organ fibrosis, and cardiomyopathy.[26-30] Beyond these effects, emerging evidence links ID to vascular calcification.[31-33] Supporting this

hypothesis, a recent study reported increased coronary artery calcification scores in CKD patients with reduced transferrin saturation.[34] Corroborating these findings, mice with metabolic syndrome on an iron-deficient diet exhibit enhanced cardiac calcification compared to those on a standard iron diet.[35] Despite these observations, the impact of ID severity on outcomes remains unclear. This study examines moderate and severe ID in two mouse models of CKD.

Methods

Mice. Male mice were used for a consistent CKD phenotype.[36,37] Mice were housed in ventilated systems (12 h dark/light, 23 ± 1 °C), fed ad libitum, and maintained on a standard diet (PicoLab Rodent Diet 20) before switching to a specialized diet. C57BL/6J mice were from Jackson Laboratory (JAX# 000664). *Col4a3*$^{-/-}$ knockout (Alport) mice were on a Sv129 background in heterozygous breeding.

Two models of CKD were used: adenine-induced nephropathy and genetic *Col4a3*$^{-/-}$ mice. Assessing iron deficiency's impact on CKD in adenine nephropathy, we established moderate and severe iron deficiency models (Figure 1A, B; Supplemental Tables 1, 2). Moderate iron deficiency was generated by feeding 8-week-old C57BL/6J mice a customized iron-deficient (4 ppm iron) 0.2% adenine-rich diet (TD.130826, Envigo) for 8 weeks. Iron-replete CKD mice were fed identical diet but with 100 ppm iron (TD.210096, Envigo). Iron-deficient and iron-replete controls were age-matched mice on an adenine-free but composition-matched diet (TD.200065, TD.80396, Envigo). Severe iron deficiency was induced by phlebotomizing 4-week-old C57BL/6J mice (~250 µl blood), and feeding them an iron-deficient diet (4 ppm iron; TD.80396, Envigo) for 4 weeks. They were then switched to a customized 0.2% adenine-rich diet that was iron-deficient (4 ppm iron; TD.130826, Envigo) for an additional 8 weeks. Matching iron-replete CKD mice were fed an iron-replete diet (100 ppm iron; TD.200065, Envigo) starting at 4 weeks of age for 4 weeks before transitioning to a customized 0.2% adenine-rich diet that was iron-replete (100 ppm iron; TD.210096, Envigo) for an additional 8 weeks. Concluding these experiments, mice were euthanized under 2.5% isoflurane, and samples were prepared as described in supplemental materials.

To assess iron deficiency's impact on CKD in a genetic model, 5-week-old Alport mice were randomly assigned to either an iron-replete (58 ppm iron; TD.80394, Envigo) or an iron-deficient diet (4 ppm iron; TD.80396, Envigo) for 5 weeks. Concluding the experiments, mice were euthanized under 2.5% isoflurane. Constitutive *Col4a3*$^{-/-}$ knockout mice are recognized as a hereditary model of human Alport syndrome, and progressive CKD. When bred on a Sv129 background, Alport mice succumb to rapid kidney injury by 10 weeks of age.

Study Approval. Animal protocols were approval by the institutional animal care and use committee of University of California, Los Angeles (UCLA).

Additional details are provided in supplemental materials.

Results

Iron deficiency models in adenine-induced CKD.

To explore the impact of iron deficiency on CKD-related complications, we generated adenine diet-induced nephropathy models with varying iron deficiency (ID) severity. Establishing effects of moderate-ID CKD mice, C57BL/6J males were fed either an iron-replete (100 ppm Fe) or iron-deficient (4 ppm Fe) diet containing 0.2% adenine for 8 weeks. Mice fed a diet lacking adenine, but with equivalent iron content, served as non-CKD iron-replete or non-CKD moderate-ID controls (Figure 1A; Supplemental Table 1). Establishing severe-ID CKD mice, C57BL/6J males were phlebotomized (~250 µL blood) by submandibular puncture and given an equal volume of saline 0.9% NaCl by intraperitoneal injection at 4 weeks of age, subjected to a 4 ppm Fe diet for 4 weeks, and transitioned to a 4 ppm Fe + 0.2% adenine diet for 8 weeks. Age-matched, non-phlebotomized mice on a 100 ppm Fe diet, later switched to a 100 ppm Fe + 0.2% adenine diet for 8 weeks, served as iron-replete CKD counterparts (Figure 1B; Supplemental Table 2). Non-CKD controls were excluded to focus on ID's effects in CKD.

We evaluated tissue and serum iron concentrations in both models to determine ID severity. Comparing non-CKD mice, liver, spleen, and heart non-heme iron levels were non-significantly decreased, and kidney iron significantly reduced in the moderate-ID model (Figure 1C-F). Transcript levels of the iron importer transferrin receptor (*Tfrc*) were slightly increased in the heart and protein (TFR1) was significantly elevated in the kidneys of non-CKD moderate-ID (Figure 1G, H), confirming tissue ID. On adenine diet, all organs (liver, heart, spleen, kidney) accumulated more iron compared to non-CKD mice with a negligible impact of moderate-ID diet on organ iron levels compared to iron-replete mice (Figure 1C-F). No differences in heart *Tfrc*

transcript and kidney TFR1 protein levels were detected between groups on adenine (Figure 1G, H). Thus, in this context of adenine-induced CKD, moderate-ID did not lead to measurable tissue iron depletion, likely resulting from CKD-related iron restriction mechanisms.

In severe-ID CKD mice, liver, spleen, heart and kidney nonheme iron levels were significantly reduced compared to iron-replete CKD mice (Figure 1C-F). This indicates that baseline tissue iron levels were profoundly diminished despite CKD-related iron restriction mechanisms. Additionally, we observed significant elevations in heart *Tfrc* transcript and kidney TFR1 protein levels in severe-ID CKD (Figure 1G, H). Interestingly, serum iron levels did not change between groups in either model (Figure 1I), likely due to reduced iron utilization for erythropoiesis following kidney injury.

Effects of moderate-ID and severe-ID on erythropoietic and hypoxic parameters in adenine-induced CKD.

Next, we assessed hematologic parameters in both models. In non-CKD controls, moderate-ID caused expected reductions in mean corpuscular volume (MCV), hemoglobin, hematocrit percentage (HCT%) and increased zinc protoporphyrin (ZPP) levels, and a trend toward increased kidney erythropoietin (*Epo*) expression (Figure 2A-E). On adenine diet, CKD mice all had anemia. However, the difference between groups was blunted or even reversed. Between moderate-ID and iron-replete CKD mice, MCV, hemoglobin, HCT%, ZPP levels and kidney *Epo* expression were similar (Figure 2A-E), indicating that moderate-ID did not worsen erythropoietic parameters beyond the effect of CKD.

In severe-ID CKD mice, MCV, ZPP and *Epo* expression levels were similar to iron-replete CKD mice as was the case for the moderate-ID group (Figure 2A, D, E), but hemoglobin and HCT% were surprisingly increased (Figure 2B, C). However, we cannot eliminate a batch effect in this experiment as CBCs in the severe-ID group were inadvertently measured on a separate day from the iron-replete group. Serum VEGF levels were significantly higher in severe-ID CKD, indicating greater systemic hypoxia in these mice, arguing against any functional improvement in the erythropoietic status of the mice (Figure 2F). Dehydration and hemoconcentration may have also contributed as total protein in serum of severe-ID CKD mice was on average 11% higher compared to iron-replete CKD. Following the normalization of hemoglobin to total serum protein for each mouse[38], severe-ID CKD and iron-replete CKD hemoglobin concentrations became similar and showed decreased variability (Figure 2G). Nevertheless, the lack of dietary ID effects on erythropoiesis in either moderate- or severe-ID CKD suggests that the anemia in this mouse model is primarily driven by CKD pathology, unlike tissue iron content in the liver, spleen, kidney and heart, which is profoundly decreased by severe-ID.

Iron deficiency aggravates systemic inflammation in adenine-induced CKD.

Inflammation is a hallmark of CKD but it is not clear whether ID directly impacts the inflammatory response in CKD. We examined hepatic and systemic inflammatory mediators in both models. In the absence of CKD, moderate-ID had no effect on cytokine expression in the liver.

Relative to non-CKD controls, iron-replete CKD mice displayed non-significant increases in liver serum amyloid A1 (*Saa1*), tumor necrosis factor α (*Tnfa*) and interleukin-6 (*Il6*) transcript levels (Figure 3A, B, D). Moderate-ID in CKD mice further elevated liver *Saa1* and *Il6* levels to statistically significant levels compared to iron-replete CKD (Figure 3A, D). No differences were observed in liver interleukin-1β (*Il1b*) mRNA expression (Figure 3C). In severe-ID CKD compared to iron-replete CKD, transcript levels of both liver *Saa1* and *Il6,* as well as serum IL-6 protein levels, were significantly elevated (Figure 3A, D, F). Notably, these levels were higher in severe-ID relative to moderate-ID mice on adenine (Figure 3A, D, F). Spleen *Il1b* transcript levels were also significantly increased in severe-ID CKD (Supplemental Figure 1B). We did not observe differences in liver *Tnfa* and *Il1b*, or spleen *Tnfa* and *Il6* transcript levels (Figure 3B, C; Supplemental Figure 1A, C).

ID suppresses hepcidin production but inflammation stimulates it.[39,40] As expected, *Hamp* transcript levels were greatly reduced (Figure 3E) and *Hamp* synthesis remained appropriately low relative to liver iron content in non-CKD moderate-ID compared to non-CKD iron-replete mice (Figure 3F). Interestingly, in the adenine model, *Hamp* transcript levels and ratios of *Hamp* synthesis relative to liver iron content were significantly and comparably elevated in both moderate-ID and iron-replete mice (Figure 3E, F), aligning with increased serum levels of the hepcidin-stimulator IL-6 (Figure 3G). Only severe-ID partially suppressed *Hamp* expression despite a strong inflammatory stimulus (Figure 3E), as evident by a significant yet inappropriately high ratio of *Hamp* synthesis relative to liver iron content in severe-ID CKD mice (Figure 3F), highlighting the opposing influences of inflammation and severe-ID on hepcidin transcription.

Since severe-ID CKD mice exhibit more pronounced systemic inflammation compared to moderate-ID CKD mice, we performed a multiplex bead immunoassay on sera from the severe-ID CKD model to gain further insight into the inflammatory milieu. Multiplex analysis of 32 cytokines and chemokines revealed significant elevations in serum TNFα and CXCL1, along with a non-significant increase in CCL4 in severe-ID CKD compared to iron-replete CKD (Figure 3H-J). Interestingly, serum CXCL2 was significantly reduced in severe-ID CKD (Figure 3K). Together, these data illustrate that the systemic inflammatory milieu in CKD is modulated by the severity of ID, which might contribute to and further aggravate CKD-associated pathologies.

Iron deficiency does not aggravate kidney injury or dysfunction in adenine-induced CKD.

Evidence suggests dietary iron restriction can improve kidney function in animal models of CKD.[41,42] We examined whether moderate-ID or severe-ID affects kidney function in our CKD model. All CKD mice displayed significant kidney dysfunction as determined by elevated blood urea nitrogen (BUN) and serum creatinine levels (Figure 4A, B) versus non-CKD controls, with no difference between ID and iron-replete (in either moderate-ID or severe-ID groups).

CKD disrupts mineral homeostasis, with ID and CKD elevating FGF23 levels, a key regulator of serum phosphate.[43-45] In non-CKD controls, moderate-ID increased FGF23 cleavage, resulting in elevated C-terminal FGF23 (cFGF23) with normal intact FGF23 (iFGF23) levels as expected (Figure 4C-E). CKD mice all had excessive levels of iFGF23 and cFGF23. However, severe-ID significantly increased FGF23 cleavage in CKD (Figure 4E). Moreover, serum phosphate was elevated in all CKD mice, unaffected by ID severity (Figure 4F).

Next, we measured kidney injury markers. All CKD groups had significantly elevated kidney neutrophil gelatinase-associated lipocalin (*Ngal*) and kidney injury marker 1 (*Kim1*) transcript levels, with no further effect from moderate- or severe-ID (Figure 4G, H). Supporting these findings, histological analysis of kidney tissue sections revealed similar pathologic alterations in all CKD mice, including pronounced tubular atrophy and dilation, along with marked interstitial inflammatory cell infiltration (Figure 4I; Supplemental Figure 1D). These data suggest that neither moderate-ID nor severe-ID impacted the severity of kidney injury or dysfunction in adenine-induced nephropathy.

Iron deficiency aggravates kidney fibrosis in adenine-induced CKD.

As our results demonstrate ID augments inflammation in CKD (Figure 3), we explored whether ID modulates kidney fibrotic progression, as inflammation is a known contributor to kidney fibrosis.[5,46] Compared to non-CKD controls, both moderate-ID CKD and iron-replete CKD mice had significantly increased kidney fibronectin (*Fn1*), transforming growth factor beta (*Tgfb*), alpha smooth muscle actin (*Acta2*), collagen type 1 alpha 1 chain (*Col1a1*) and collagen type 3 alpha 1 chain (*Col3a1*) transcript levels (Figure 5A-E). Interestingly, *Col3a1* transcript levels were significantly increased in moderate-ID CKD compared to iron-replete CKD (Figure 5E). Severe-ID CKD likewise potentiated mRNA expression of kidney *Acta2*, *Col1a1* and *Col3a1* compared to iron-replete CKD counterparts (Figure 5C-E). Histopathological analysis of kidney tissue sections revealed extensive collagen deposition in both the glomeruli and interstitium across CKD groups, but particularly potentiated in severe-ID CKD mice (Figure 5F;

Supplemental Figure 1E). Taken together, these results indicate that ID aggravates kidney fibrotic progression in adenine-induced nephropathy.

Iron deficiency does not aggravate kidney tissue inflammation or calcification in adenine-induced CKD.

Next, we examined ID's role in kidney calcification by analyzing local inflammatory cytokine expression, which triggers calcification pathways.[47] Kidney *Tnfa* and *Il6* transcript levels were similarly elevated in moderate-ID and iron-replete mice on adenine, versus controls (Supplemental Figure 2A, B). Measuring expression of calcification genes, kidney runt related transcription factor 2 (*Runx2*), sex determining region-box 9 (*Sox9*), and osteopontin (*Opn*) transcript levels were significantly and similarly elevated in moderate-ID and iron-replete mice on adenine (Supplemental Figure 2C-E).

In severe-ID CKD mice, kidney *Tnfa*, *Il6*, *Runx2*, *Sox9*, or *Opn* levels showed no significant differences from iron-replete CKD mice (Supplemental Figure 2). Thus, ID neither potentiates kidney tissue inflammation nor contributes to the pathogenesis of kidney calcification in adenine-induced CKD.

Iron deficiency does not aggravate cardiovascular inflammation or calcification in adenine-induced CKD.

Vascular calcification stiffens arteries, exacerbating hypertension, heart failure and mortality, particularly in CKD.[10,48] We investigated ID's role in cardiac calcification by assessing inflammation. Cardiac *Tnfa* mRNA showed a non-significant increase in both moderate-ID and iron-replete CKD mice versus controls (Supplemental Figure 3A). We observed no changes in

cardiac *Il1b* or *Il6* transcript levels (Supplemental Figure 3B, C). Measuring expression of calcification genes, cardiac *Runx2, Sox9* and *Opn* transcript levels were significantly and uniformly elevated in both moderate-ID and iron-replete mice on adenine (Supplemental Figure 3D-F). These data indicate that although cardiac inflammation was mild, signaling pathways involved in cardiovascular calcification were activated in adenine-induced CKD, but unaffected by moderate-ID.

In severe-ID CKD mice, cardiac *Tnfa, Il1b, Il6, Runx2, Sox9,* and *Opn* levels showed no significant differences from iron-replete CKD mice (Supplemental Figure 3). These data confirm that ID does not affect cardiac inflammation or calcification in adenine-induced CKD.

Iron deficiency does not aggravate CKD-associated cardiomyopathy in adenine nephropathy.

Given that systemic inflammation and anemia are risk factors for heart disease, we explored whether ID impacts cardiac injury and/or fibrosis. Cardiac hypertrophy, indicated by heart-to-body weight ratio, was present in moderate-ID and iron-replete CKD mice versus controls (Figure 6A). Furthermore, mRNA expression of cardiac adult alpha-myosin heavy chain (*Myh6*) was significantly and similarly reduced, whereas fetal beta-myosin heavy chain (*Myh7*) was significantly and similarly increased in both moderate-ID and iron-replete CKD mice (Figure 6B, C). The transition from adult to fetal myosin heavy chain isoforms signifies the reactivation of fetal gene programs related to cardiac hypertrophy.[49-52] Additionally, cardiac fibrosis was observed in both moderate-ID and iron-replete CKD mice, as evidenced by marked and uniformly elevated cardiac *Tgfb* and *Col1a1* transcript levels, corroborated by histopathological analysis of heart tissue sections revealing consistent collagen deposition within the myocardium

(Figure 6D, E, G; Supplemental Figure 1F). No changes were observed in cardiac *Acta2* mRNA expression (Figure 6F).

Evaluating pathologic cardiac remodeling in severe-ID CKD mice, heart-to-body weight ratio and mRNA expression of cardiac *Myh6* and *Myh7* reflected similar cardiac hypertrophy between severe-ID CKD and iron-replete CKD mice (Figure 6A-C). However, severe-ID amplified the expression of *Tgfb*, *Col1a1*, and *Acta2* (Figure 6D-F), resulting in a modest, albeit non-significant, increase in myocardial collagen deposition (Figure 6G), indicating a slight worsening of myocardial fibrosis. Collectively, these data demonstrate that the severity of ID does aggravate the expression of cardiac fibrosis markers, but without substantially impacting CKD-associated cardiomegaly.

Iron deficiency does not aggravate CKD-associated pathologies in Alport (Col4a3$^{-/-}$) mice.

Examining these findings in a genetic CKD model, we utilized Alport (*Col4a3*$^{-/-}$) mice, which develop progressive CKD with systemic inflammation, mild ID and anemia,[53,54] as well as kidney and cardiovascular dysfunction with concurrent fibrosis.[37,54] Testing if ID worsens these complications, we generated moderate-ID in *Col4a3*$^{-/-}$ mice by subjecting males to an iron-deficient (4 ppm Fe) diet for 5 weeks (Supplemental Figure 4A). In comparison to *Col4a3*$^{-/-}$ mice fed an iron-replete (58 ppm Fe) diet, moderate-ID *Col4a3*$^{-/-}$ mice displayed increased kidney TFR1 protein levels, and reduced kidney iron, serum iron, MCV, hemoglobin, and HCT% (Supplemental Figures 4D, F, G and 5A-C), consistent with expected effects of moderate systemic ID.

We next explored the impact of moderate-ID on CKD-associated complications in the Alport model. We detected no substantial alterations in systemic inflammation (Supplemental

Figure 6) but increased kidney *Tnfa*, (Supplemental Figure 9A). There was no effect of moderate-ID on kidney injury or dysfunction (Supplemental Figure 7), kidney fibrosis (Supplemental Figure 8), kidney inflammation and calcification (Supplemental Figure 9), cardiovascular inflammation and calcification (Supplemental Figure 10), or pathologic cardiac remodeling, with the exception of increased *Acta2* expression in the heart of iron-deficient animals (Supplemental Figure 11). Taken together, these data indicate that moderate-ID does not strongly modulate CKD-associated complications in Alport mice, despite impairing erythropoiesis in this model.

Discussion

Over 180 years ago, anemia was first connected to CKD.[55] Today, numerous studies confirm the widespread prevalence of iron deficiency (ID) and anemia in these patients, and these conditions have been associated with CKD progression, organ fibrosis, vascular calcification, and cardiomyopathy.[26-28,34] Impairment of hemoglobin synthesis is a relatively late consequence of ID, with anemia only manifesting in a third of iron-deficient individuals.[56] Furthermore, ID can have adverse effects on cell and tissue function independently of the effects of anemia. Thus, understanding the pathologic consequences of ID in CKD can help optimize iron supplementation strategies to improve outcomes both by correcting tissue ID and by improving anemia. The present study directly assesses the impact of different degrees of ID on common CKD-associated complications using mouse models. Utilizing both dietary-induced and genetic mouse models of CKD, we induced moderate or severe-ID, and examined a broad array of potential effects. We demonstrate that although ID does not modulate vascular calcification, kidney injury, kidney dysfunction, or pathological cardiac remodeling, ID does potentiate

systemic inflammation, as well as kidney and cardiac fibrosis. These effects appear independent of anemia in the adenine model, as erythropoietic parameters were not worsened by either moderate or severe ID. It appears that in the setting of CKD, where erythropoiesis is suppressed from the effects of renal toxins and systemic inflammation, ID, even if severe, has much less effect on the erythron (Figure 2) compared to non-erythroid tissues (Figure 1).

In the CKD group with moderate-ID, where mice were fed a low-iron diet, neither tissue iron levels nor erythroid parameters differed from those of the iron-replete CKD group receiving 100 ppm iron. Although initially puzzling, this can likely be attributed to hepcidin-mediated iron restriction resulting from functional ID in adenine-induced CKD. As a result, even mice receiving 100 ppm iron were unable to effectively utilize dietary iron, rendering both groups similarly iron deficient/restricted. It is therefore not surprising that we observed small or no differences in CKD complications between the two groups given that they differed little in their iron or erythropoietic status. The second ID model we used (severe-ID), which relied on lowering iron stores through phlebotomy prior to the onset of CKD, allowed us to examine the effect of true tissue ID on CKD pathology. Interestingly, compared to their non-CKD counterparts, moderate-ID CKD mice had significantly higher iron accumulation observed in the liver, spleen, heart, and kidney. This is likely the consequence of iron being redistributed from the erythroid/RBC compartment to other tissues, both because of decreased utilization of iron by nascent erythropoiesis, and because of accelerated destruction of mature RBCs.

Clinical studies have reported persistent inflammation, even at low to moderate levels, exacerbates CKD-related comorbidities.[57-59] However, the effects of ID on chronic inflammation remain poorly characterized. In our study, severe-ID intensified the systemic inflammatory milieu, as severe-ID CKD mice displayed increased liver and splenic inflammatory markers and

elevated plasma cytokines compared to iron-replete CKD mice (Figure 3; Supplemental Figure 1). Even the moderate-ID CKD group had more liver inflammation, as reflected by higher *Saa1* (Figure 3). Furthermore, we detected increased circulating TNFα levels in severe-ID CKD mice (Figure 3). Given that TNFα is known to exacerbate anemia[60-62], its upregulation in our adenine model may potentiate the effects of ID, creating a self-perpetuating cycle that amplifies systemic inflammation. This heightened inflammatory milieu could further drive the activation and recruitment of inflammatory cells, such as neutrophils and macrophages, to affected tissues. Such mechanisms could aggravate CKD-associated pathologies. Supporting this postulate, a recent report demonstrates that iron dextran administration in CKD blunts the production of pro-inflammatory cytokines.[26] Although our Alport (*Col4a3*$^{-/-}$) mice fed an iron-replete diet displayed increased inflammation relative to adenine-fed mice, moderate-ID in Alport mice did not amplify systemic inflammation (Supplemental Figure 4-6). These findings suggest that while ID can augment the inflammatory milieu in CKD, it may not contribute further when the inflammatory response is already highly activated.

Inflammation and ID are also commonly associated with fibrotic development in CKD, although a recent study suggests fibrosis may arise independently of inflammation.[63] In our analysis of the adenine model, severe-ID—resulting in profound iron depletion across multiple tissues—exacerbated kidney fibrotic gene expression and interstitial fibrosis, despite similar expression of markers of kidney injury, impaired kidney function, and kidney tissue inflammation when compared to iron-replete CKD mice (Figures 4, 5; Supplemental Figure 2). A plausible mechanism explaining our data might involve intracellular ID in kidney macrophages, where it is reported to drive a profibrotic phenotype in CKD.[26] While moderate-ID did not aggravate this profibrotic response, it also failed to further intensify tissue ID relative to

iron-replete CKD. However, in the context of severe-ID, CKD mice also exhibited increased systemic levels of fibrotic-associated cytokines CXCL1 and CCL4, compared to iron-replete CKD mice (Figure 3). It is also possible that severe-ID may contribute to worse CKD by precipitating a more severe acute kidney injury after the initial exposure to adenine.

Given that CXCL1 promotes fibrosis by recruiting immune cells to injured tissues and CCL4 contributes to oxidative stress, fibroblast activation, and immune cell recruitment[64-67], coupled with iron's critical role in immune cell function[68], we hypothesize that ID induces distinct metabolic reprogramming of kidney immune cells relative to other tissues. Consequently, this metabolic rewiring augments the sensitivity of kidney immune cells to inflammatory stimuli, thereby amplifying their profibrotic activity. Similarly, in the heart, severe-ID potentiated expression of multiple fibrotic markers in adenine-CKD, while moderate-ID elevated *Acta2* expression in Alport mice (Figure 6; Supplemental Figures 10, 11). This suggests potential similarities in metabolic rewiring between the kidney and the heart in response to different levels of ID. Nonetheless, additional studies are required to test this hypothesis.

Beyond its role in fibrosis, ID may also contribute to cardiovascular complications in CKD, particularly by modulating vascular calcification. While vascular calcification is a major driver of cardiovascular mortality in CKD,[48,69,70] the impact of ID on cardiac injury—especially through its effects on kidney and cardiac calcification—remains largely unexplored. Although few studies directly suggest that ID influences vascular calcification,[31-33] our findings indicate that the pathogenesis of heart failure occurs independently of ID-induced changes in kidney and cardiac calcification (Supplemental Figures 2, 3, 9, 10). Furthermore, we observed no significant ID-attributable differences in heart injury across both CKD models (Figure 6; Supplemental Figure 11). However, we did not directly examine cardiomyocyte intracellular ID or

mitochondrial dysfunction, both of which are known to be associated with impaired cardiac function.[71]

This study has several strengths. By utilizing both an adenine-induced nephropathy model and a genetic *Col4a3*$^{-/-}$ (Alport) model, we provide a comprehensive assessment of models of CKD pathology. Additionally, we established different gradations of ID, enabling a nuanced understanding of how different degrees of ID impact CKD. This approach better reflects heterogeneity observed in human CKD patients. However, this study also has notable limitations. First, only male mice were used, as they exhibit a consistent CKD phenotype. While this choice is common in the field, it limits generalizability of our findings to females. Second, adenine model is prone to inducing a severe, often lethal CKD phenotype. Given that ID did not exacerbate kidney injury despite presence of extensive fibrotic lesions following 8-weeks of adenine, a time-course evaluation could help clarify whether ID accelerates kidney injury at earlier stages compared to iron-replete conditions. Third, rapid progression of kidney injury in Alport mice leads to mortality by 10 weeks of age, thus a 5-week 4ppm Fe diet may not fully capture long-term effects of moderate-ID in this model. Lastly, while we assessed cardiac fibrosis, we did not evaluate functional cardiac parameters, leaving this aspect of CKD-related cardiac effects unexplored.

In conclusion, our study establishes models of moderate and severe ID in adenine nephropathy as well as moderate ID in Alport mice. We found that ID amplifies systemic inflammation and worsens both kidney and cardiac fibrosis, particularly in adenine-induced CKD. Notably, ID did not affect other CKD-related complications, including kidney injury and dysfunction, vascular calcification, or cardiomyopathy, in either model. Our data suggests that iron supplementation may be beneficial to combat inflammation-induced kidney damage, and

offers a more comprehensive understanding of its therapeutic potential. Future studies exploring targeted iron supplementation strategies to mitigate kidney and cardiac fibrosis in CKD complicated with ID are warranted to translate these findings into clinical practice.

Acknowledgments

The authors acknowledge financial support from the National Institutes of Health: K01-DK-127004 (VS), IK2-CX-002195 (SS), R01-DK-126680 (TG), R01-DK-136691 (EN), and T32-HL-072752 (BC). We greatly appreciate the support of UCLA's Integrated Molecular Technologies Core and Translational Pathology Core Laboratory for their expertise in conducting the serum 32-plex cytokine/chemokine immunoassay and tissue processing/staining for histopathological analysis.

Author Contributions

MZ and AL performed experiments and analyzed data. GJ, JO, VS assisted with experiments. SS, TG, EN, MH helped conceive and plan the project, and assisted with data interpretation and manuscript editing. BC conceived the project, designed and performed experiments, analyzed

data, prepared figures, and wrote the manuscript. All authors discussed results, read and contributed edits to manuscript, and approved final version.

Disclosure of Conflicts of Interest

The authors declare competing financial interests: TG and EN are shareholders and scientific advisers of Intrinsic LifeSciences and Silarus Therapeutics, and consultants for Disc Medicine, Ionis Pharmaceuticals, Protagonist, Vifor, GSK, Chiesi, Novo Nordisk (EN), Silence Therapeutics, Intrinsic LifeSciences. Ionis Pharmaceuticals, Disc Medicine, City Therapeutics, Chugai, Dexcel, BristolMyersSquib (TG). Other authors report no conflict of interest.

References

1. Francis A, Harhay MN, Ong ACM, et al. Chronic kidney disease and the global public health agenda: an international consensus. *Nat Rev Nephrol*. 2024;20(7):473-485.
2. Webster AC, Nagler EV, Morton RL, Masson P. Chronic Kidney Disease. *Lancet*. 2017;389(10075):1238-1252.
3. Chesnaye NC, Ortiz A, Zoccali C, Stel VS, Jager KJ. The impact of population ageing on the burden of chronic kidney disease. *Nat Rev Nephrol*. 2024;20(9):569-585.
4. Kidney Disease: Improving Global Outcomes CKDWG. KDIGO 2024 Clinical Practice Guideline for the Evaluation and Management of Chronic Kidney Disease. *Kidney Int*. 2024;105(4S):S117-S314.
5. Black LM, Lever JM, Agarwal A. Renal Inflammation and Fibrosis: A Double-edged Sword. *J Histochem Cytochem*. 2019;67(9):663-681.
6. Chiuariu T, Salaru D, Ureche C, et al. Cardiac and Renal Fibrosis, the Silent Killer in the Cardiovascular Continuum: An Up-to-Date. *J Cardiovasc Dev Dis*. 2024;11(2).
7. Dai L, Schurgers LJ, Shiels PG, Stenvinkel P. Early vascular ageing in chronic kidney disease: impact of inflammation, vitamin K, senescence and genomic damage. *Nephrol Dial Transplant*. 2020;35(Suppl 2):ii31-ii37.
8. Hoshino J, Muenz D, Zee J, et al. Associations of Hemoglobin Levels With Health-Related Quality of Life, Physical Activity, and Clinical Outcomes in Persons With Stage 3-5 Nondialysis CKD. *J Ren Nutr*. 2020;30(5):404-414.
9. Hwang IC, Park HE, Kim HL, et al. Systemic Inflammation Is Associated With Coronary Artery Calcification and All-Cause Mortality in Chronic Kidney Disease. *Circ J*. 2016;80(7):1644-1652.
10. Go AS, Chertow GM, Fan D, McCulloch CE, Hsu CY. Chronic kidney disease and the risks of death, cardiovascular events, and hospitalization. *N Engl J Med*. 2004;351(13):1296-1305.

11. Drakesmith H, Pasricha SR, Cabantchik I, et al. Vaccine efficacy and iron deficiency: an intertwined pair? *Lancet Haematol*. 2021;8(9):e666-e669.
12. Li Y, Shi H, Wang WM, et al. Prevalence, awareness, and treatment of anemia in Chinese patients with nondialysis chronic kidney disease: First multicenter, cross-sectional study. *Medicine (Baltimore)*. 2016;95(24):e3872.
13. St Peter WL, Guo H, Kabadi S, et al. Prevalence, treatment patterns, and healthcare resource utilization in Medicare and commercially insured non-dialysis-dependent chronic kidney disease patients with and without anemia in the United States. *BMC Nephrol*. 2018;19(1):67.
14. Palaka E, Grandy S, van Haalen H, McEwan P, Darlington O. The Impact of CKD Anaemia on Patients: Incidence, Risk Factors, and Clinical Outcomes-A Systematic Literature Review. *Int J Nephrol*. 2020;2020:7692376.
15. van Nooten FE, Green J, Brown R, Finkelstein FO, Wish J. Burden of illness for patients with non-dialysis chronic kidney disease and anemia in the United States: review of the literature. *J Med Econ*. 2010;13(2):241-256.
16. Babitt JL, Lin HY. Mechanisms of anemia in CKD. *J Am Soc Nephrol*. 2012;23(10):1631-1634.
17. Babitt JL, Eisenga MF, Haase VH, et al. Controversies in optimal anemia management: conclusions from a Kidney Disease: Improving Global Outcomes (KDIGO) Conference. *Kidney Int*. 2021;99(6):1280-1295.
18. Nemeth E, Rivera S, Gabayan V, et al. IL-6 mediates hypoferremia of inflammation by inducing the synthesis of the iron regulatory hormone hepcidin. *J Clin Invest*. 2004;113(9):1271-1276.
19. Kanamori Y, Murakami M, Sugiyama M, Hashimoto O, Matsui T, Funaba M. Interleukin-1beta (IL-1beta) transcriptionally activates hepcidin by inducing CCAAT enhancer-binding protein delta (C/EBPdelta) expression in hepatocytes. *J Biol Chem*. 2017;292(24):10275-10287.
20. Nemeth E, Tuttle MS, Powelson J, et al. Hepcidin regulates cellular iron efflux by binding to ferroportin and inducing its internalization. *Science*. 2004;306(5704):2090-2093.
21. Batchelor EK, Kapitsinou P, Pergola PE, Kovesdy CP, Jalal DI. Iron Deficiency in Chronic Kidney Disease: Updates on Pathophysiology, Diagnosis, and Treatment. *J Am Soc Nephrol*. 2020;31(3):456-468.
22. Gafter-Gvili A, Schechter A, Rozen-Zvi B. Iron Deficiency Anemia in Chronic Kidney Disease. *Acta Haematol*. 2019;142(1):44-50.
23. Macdougall IC. Anaemia in CKD-treatment standard. *Nephrol Dial Transplant*. 2024;39(5):770-777.
24. Kovesdy CP, Trivedi BK, Kalantar-Zadeh K, Anderson JE. Association of anemia with outcomes in men with moderate and severe chronic kidney disease. *Kidney Int*. 2006;69(3):560-564.
25. Thorp ML, Johnson ES, Yang X, Petrik AF, Platt R, Smith DH. Effect of anaemia on mortality, cardiovascular hospitalizations and end-stage renal disease among patients with chronic kidney disease. *Nephrology (Carlton)*. 2009;14(2):240-246.
26. Patino E, Bhatia D, Vance SZ, et al. Iron therapy mitigates chronic kidney disease progression by regulating intracellular iron status of kidney macrophages. *JCI Insight*. 2023;8(1).
27. Saraf SL, Hsu JY, Ricardo AC, et al. Anemia and Incident End-Stage Kidney Disease. *Kidney360*. 2020;1(7):623-630.

28. Ezekowitz JA, McAlister FA, Armstrong PW. Anemia is common in heart failure and is associated with poor outcomes: insights from a cohort of 12 065 patients with new-onset heart failure. *Circulation*. 2003;107(2):223-225.
29. Anand IS, Kuskowski MA, Rector TS, et al. Anemia and change in hemoglobin over time related to mortality and morbidity in patients with chronic heart failure: results from Val-HeFT. *Circulation*. 2005;112(8):1121-1127.
30. Anand IS. Anemia and chronic heart failure implications and treatment options. *J Am Coll Cardiol*. 2008;52(7):501-511.
31. Ciceri P, Elli F, Braidotti P, et al. Iron citrate reduces high phosphate-induced vascular calcification by inhibiting apoptosis. *Atherosclerosis*. 2016;254:93-101.
32. Ciceri P, Falleni M, Tosi D, et al. High-phosphate induced vascular calcification is reduced by iron citrate through inhibition of extracellular matrix osteo-chondrogenic shift in VSMCs. *Int J Cardiol*. 2019;297:94-103.
33. Seto T, Hamada C, Tomino Y. Suppressive effects of iron overloading on vascular calcification in uremic rats. *J Nephrol*. 2014;27(2):135-142.
34. Mizuiri S, Nishizawa Y, Doi T, et al. Iron, coronary artery calcification, and mortality in patients undergoing hemodialysis. *Ren Fail*. 2021;43(1):371-380.
35. Naito Y, Sawada H, Yasumura S, et al. Iron Deficiency Induces Heart Failure With Ectopic Cardiac Calcification in Mice With Metabolic Syndrome. *Circ Heart Fail*. 2022;15(7):e009034.
36. Diwan V, Small D, Kauter K, Gobe GC, Brown L. Gender differences in adenine-induced chronic kidney disease and cardiovascular complications in rats. *Am J Physiol Renal Physiol*. 2014;307(11):F1169-1178.
37. Neuburg S, Dussold C, Gerber C, et al. Genetic background influences cardiac phenotype in murine chronic kidney disease. *Nephrol Dial Transplant*. 2018;33(7):1129-1137.
38. McNulty SE, Sharkey SJ, Schieren H. Bedside hemoglobin measurements: sensitivity to changes in serum protein and electrolytes. *J Clin Monit*. 1994;10(6):377-381.
39. Kautz L, Jung G, Valore EV, Rivella S, Nemeth E, Ganz T. Identification of erythroferrone as an erythroid regulator of iron metabolism. *Nat Genet*. 2014;46(7):678-684.
40. Nemeth E, Valore EV, Territo M, Schiller G, Lichtenstein A, Ganz T. Hepcidin, a putative mediator of anemia of inflammation, is a type II acute-phase protein. *Blood*. 2003;101(7):2461-2463.
41. Naito Y, Fujii A, Sawada H, et al. Effect of iron restriction on renal damage and mineralocorticoid receptor signaling in a rat model of chronic kidney disease. *J Hypertens*. 2012;30(11):2192-2201.
42. Naito Y, Fujii A, Sawada H, et al. Dietary iron restriction prevents further deterioration of renal damage in a chronic kidney disease rat model. *J Hypertens*. 2013;31(6):1203-1213.
43. Farrow EG, Yu X, Summers LJ, et al. Iron deficiency drives an autosomal dominant hypophosphatemic rickets (ADHR) phenotype in fibroblast growth factor-23 (Fgf23) knock-in mice. *Proc Natl Acad Sci U S A*. 2011;108(46):E1146-1155.
44. Martin A, David V, Quarles LD. Regulation and function of the FGF23/klotho endocrine pathways. *Physiol Rev*. 2012;92(1):131-155.
45. Wolf M, Molnar MZ, Amaral AP, et al. Elevated fibroblast growth factor 23 is a risk factor for kidney transplant loss and mortality. *J Am Soc Nephrol*. 2011;22(5):956-966.
46. Reiss AB, Jacob B, Zubair A, Srivastava A, Johnson M, De Leon J. Fibrosis in Chronic Kidney Disease: Pathophysiology and Therapeutic Targets. *J Clin Med*. 2024;13(7).

47. Kawtharany L, Bessueille L, Issa H, Hamade E, Zibara K, Magne D. Inflammation and Microcalcification: A Never-Ending Vicious Cycle in Atherosclerosis? *J Vasc Res*. 2022;59(3):137-150.
48. London GM, Guerin AP, Marchais SJ, Metivier F, Pannier B, Adda H. Arterial media calcification in end-stage renal disease: impact on all-cause and cardiovascular mortality. *Nephrol Dial Transplant*. 2003;18(9):1731-1740.
49. Morkin E. Control of cardiac myosin heavy chain gene expression. *Microsc Res Tech*. 2000;50(6):522-531.
50. Izumo S, Lompre AM, Matsuoka R, et al. Myosin heavy chain messenger RNA and protein isoform transitions during cardiac hypertrophy. Interaction between hemodynamic and thyroid hormone-induced signals. *J Clin Invest*. 1987;79(3):970-977.
51. Molkentin JD, Lu JR, Antos CL, et al. A calcineurin-dependent transcriptional pathway for cardiac hypertrophy. *Cell*. 1998;93(2):215-228.
52. Faul C, Amaral AP, Oskouei B, et al. FGF23 induces left ventricular hypertrophy. *J Clin Invest*. 2011;121(11):4393-4408.
53. Czaya B, Heitman K, Campos I, et al. Hyperphosphatemia increases inflammation to exacerbate anemia and skeletal muscle wasting independently of FGF23-FGFR4 signaling. *Elife*. 2022;11.
54. Francis C, Courbon G, Gerber C, et al. Ferric citrate reduces fibroblast growth factor 23 levels and improves renal and cardiac function in a mouse model of chronic kidney disease. *Kidney Int*. 2019;96(6):1346-1358.
55. Cases and Observations Illustrative of Renal Disease, Accompanied with the Secretion of Albuminous Urine. *Med Chir Rev*. 1836;25(49):23-35.
56. Camaschella C. Iron deficiency. *Blood*. 2019;133(1):30-39.
57. Kimmel PL, Phillips TM, Simmens SJ, et al. Immunologic function and survival in hemodialysis patients. *Kidney Int*. 1998;54(1):236-244.
58. Dregan A, Charlton J, Chowienczyk P, Gulliford MC. Chronic inflammatory disorders and risk of type 2 diabetes mellitus, coronary heart disease, and stroke: a population-based cohort study. *Circulation*. 2014;130(10):837-844.
59. Guarner V, Rubio-Ruiz ME. Low-grade systemic inflammation connects aging, metabolic syndrome and cardiovascular disease. *Interdiscip Top Gerontol*. 2015;40:99-106.
60. La Ferla K, Reimann C, Jelkmann W, Hellwig-Burgel T. Inhibition of erythropoietin gene expression signaling involves the transcription factors GATA-2 and NF-kappaB. *FASEB J*. 2002;16(13):1811-1813.
61. Moldawer LL, Marano MA, Wei H, et al. Cachectin/tumor necrosis factor-alpha alters red blood cell kinetics and induces anemia in vivo. *FASEB J*. 1989;3(5):1637-1643.
62. Rusten LS, Jacobsen SE. Tumor necrosis factor (TNF)-alpha directly inhibits human erythropoiesis in vitro: role of p55 and p75 TNF receptors. *Blood*. 1995;85(4):989-996.
63. Maarouf OH, Aravamudhan A, Rangarajan D, et al. Paracrine Wnt1 Drives Interstitial Fibrosis without Inflammation by Tubulointerstitial Cross-Talk. *J Am Soc Nephrol*. 2016;27(3):781-790.
64. Chang TT, Lin LY, Chen C, Chen JW. CCL4 contributes to aging related angiogenic insufficiency through activating oxidative stress and endothelial inflammation. *Angiogenesis*. 2024;27(3):475-499.
65. Li R, Frangogiannis NG. Chemokines in cardiac fibrosis. *Curr Opin Physiol*. 2021;19:80-91.

66. Wu CL, Yin R, Wang SN, Ying R. A Review of CXCL1 in Cardiac Fibrosis. *Front Cardiovasc Med*. 2021;8:674498.
67. Zhou C, Gao Y, Ding P, Wu T, Ji G. The role of CXCL family members in different diseases. *Cell Death Discov*. 2023;9(1):212.
68. Frost JN, Wideman SK, Preston AE, et al. Plasma iron controls neutrophil production and function. *Sci Adv*. 2022;8(40):eabq5384.
69. Eckardt KU, Coresh J, Devuyst O, et al. Evolving importance of kidney disease: from subspecialty to global health burden. *Lancet*. 2013;382(9887):158-169.
70. Mukai H, Dai L, Chen Z, et al. Inverse J-shaped relation between coronary arterial calcium density and mortality in advanced chronic kidney disease. *Nephrol Dial Transplant*. 2020;35(7):1202-1211.
71. van der Wal HH, Grote Beverborg N, Dickstein K, et al. Iron deficiency in worsening heart failure is associated with reduced estimated protein intake, fluid retention, inflammation, and antiplatelet use. *Eur Heart J*. 2019;40(44):3616-3625.

Figure Legends

Figure 1. Generation of graded iron-deficient models in adenine-induced CKD.

(**A-B**) Schematic of moderate (A) and severe (B) -iron deficiency (ID) models in mice fed iron-replete (100 ppm; Fe) or iron-deficient (4 ppm; -Fe) diets, with or without 0.2% adenine to induce CKD. Non-heme iron levels in liver (**C**), spleen (**D**), heart (**E**) and kidney (**F**) tissue. (**G**) Quantitative PCR (qPCR) analysis of *Tfrc* expression in heart tissue. (**H**) Densitometry of TFR1 protein levels in kidney tissue. (**I**) Serum iron levels. Data are mean ± SEM (n = 4–8 mice/group; *$p \leq 0.05$ vs. Fe + control, #$p \leq 0.05$ vs. -Fe + control; n = 8 mice/group; $^{\alpha}p \leq 0.05$ vs. Fe + CKD) analyzed by two-way analysis of variance (ANOVA) with Tukey post hoc test for moderate-ID, or unpaired-*t*-test with Welch's correction (two-tailed) for severe-ID.

Figure 2. Effects of iron deficiency on complete blood count parameters, kidney erythropoietin and serum VEGF levels in adenine-induced CKD.

Moderate and severe-ID models in mice fed iron-replete (100 ppm; Fe) or iron-deficient (4 ppm; -Fe) diets, with or without 0.2% adenine to induce CKD. Measured parameters include (**A**) mean corpuscular volume (MCV), (**B**) hemoglobin, (**C**) hematocrit percentage (HCT%), (**D**) zinc protoporphyrin (ZPP), (**E**) qPCR analysis of *Epo* expression in kidney tissue, (**F**) serum VEGF levels, and (**G**) hemoglobin relative to serum total protein levels. Data are mean ± SEM (n = 4–5 mice/group; *$p \leq 0.05$ vs. Fe + control, #$p \leq 0.05$ vs. -Fe + control; n = 8 mice/group; $^{\alpha}p \leq 0.05$ vs. Fe + CKD) analyzed by two-way ANOVA with Tukey post hoc test for moderate-ID, or unpaired-*t*-test with Welch's correction (two-tailed) for severe-ID.

Figure 3. Iron deficiency exacerbates systemic inflammation in adenine-induced CKD.

Moderate and severe-ID models in mice fed iron-replete (100 ppm; Fe) or iron-deficient (4 ppm; -Fe) diets, with or without 0.2% adenine to induce CKD. qPCR analysis of *Saa1* (**A**), *Tnfa* (**B**), *Il1b* (**C**), *Il6* (**D**) and *Hamp* (**E**) expression in liver tissue. (**F**) Liver *Hamp*/liver iron content ratio. (**G**) Serum IL-6 levels. (**H-K**) Serum 32-plex cytokine/chemokine analysis in the severe-ID model. Data are mean ± SEM (n = 4–7 mice/group; *$p \leq 0.05$ vs. Fe + control, #$p \leq 0.05$ vs. -Fe + control; n = 7-8 mice/group; $^{\alpha}p \leq 0.05$ vs. Fe + CKD) analyzed by two-way ANOVA with Tukey post hoc test for moderate-ID, or unpaired-*t*-test with Welch's correction (two-tailed) for severe-ID.

Figure 4. Iron deficiency does not exacerbate kidney injury, dysregulated mineral metabolism or functional impairment in adenine-induced CKD.

Moderate and severe-ID models in mice fed iron-replete (100 ppm; Fe) or iron-deficient (4 ppm; -Fe) diets, with or without 0.2% adenine to induce CKD. Measured parameters include (**A**) blood urea nitrogen (BUN), (**B**) serum creatinine, (**C**) serum intact FGF23, (**D**) serum c-terminal FGF23 (**E**) intact FGF23 relative to c-terminal FGF23, and (**F**) serum phosphate. qPCR analysis of *Ngal* (**G**) and *Kim1* (**H**) expression in kidney tissue. (**I**) Representative H&E-stained kidney sections (10x magnification, scale bar, 200 um; 40x magnification, scale bar, 50 um). Data are mean ± SEM (n = 4–7 mice/group; *p ≤ 0.05 vs. Fe + control, #p ≤ 0.05 vs. -Fe + control; n = 7-8 mice/group; $^{\alpha}$p ≤ 0.05 vs. Fe + CKD) analyzed by two-way ANOVA with Tukey post hoc test for moderate-ID, or unpaired-*t*-test with Welch's correction (two-tailed) for severe-ID.

Figure 5. Iron deficiency exacerbates kidney fibrosis in adenine-induced CKD.

Moderate and severe-ID models in mice fed iron-replete (100 ppm; Fe) or iron-deficient (4 ppm; -Fe) diets, with or without 0.2% adenine to induce CKD. qPCR analysis of *Fn1* (**A**), *Tgfb* (**B**), *Acta2* (**C**), *Col1a1* (**D**) and *Col3a1* (**E**) expression in kidney tissue. (**F**) Representative Masson's trichrome-stained kidney sections with quantification shown as fibrosis score; n=5 mice/group (10x magnification, scale bar, 200 um; 40x magnification, scale bar, 50 um). Data are mean ± SEM (n = 4–7 mice/group; *p ≤ 0.05 vs. Fe + control, #p ≤ 0.05 vs. -Fe + control, $p ≤ 0.05 vs. Fe + CKD; n = 7-8 mice/group; $^{\alpha}$p ≤ 0.05 vs. Fe + CKD) analyzed by two-way ANOVA with Tukey post hoc test for moderate-ID, or unpaired-*t*-test with Welch's correction (two-tailed) for severe-ID.

Figure 6. Iron deficiency does not exacerbate cardiac injury but potentiates expression of cardiac markers of fibrosis in adenine-induced CKD.

Moderate and severe-ID models in mice fed iron-replete (100 ppm; Fe) or iron-deficient (4 ppm; -Fe) diets, with or without 0.2% adenine to induce CKD. (**A**) Heart weight relative to body weight. qPCR analysis of *Myh6* (**B**), *Myh7* (**C**), *Tgfb* (**D**), *Col1a1* (**E**), and *Acta2* (**F**) expression in heart tissue. (**G**) Representative Masson's trichrome-stained heart sections with quantification shown as fibrosis score; n=5 mice/group (original magnification, 10x; scale bar, 200 μm). Data are mean ± SEM (n = 4–7 mice/group; *$p \leq 0.05$ vs. Fe + control, #$p \leq 0.05$ vs. -Fe + control; n = 8 mice/group; $^{\alpha}p \leq 0.05$ vs. Fe + CKD) analyzed by two-way ANOVA with Tukey post hoc test for moderate-ID, or unpaired-*t*-test with Welch's correction (two-tailed) for severe-ID.

Figure 1

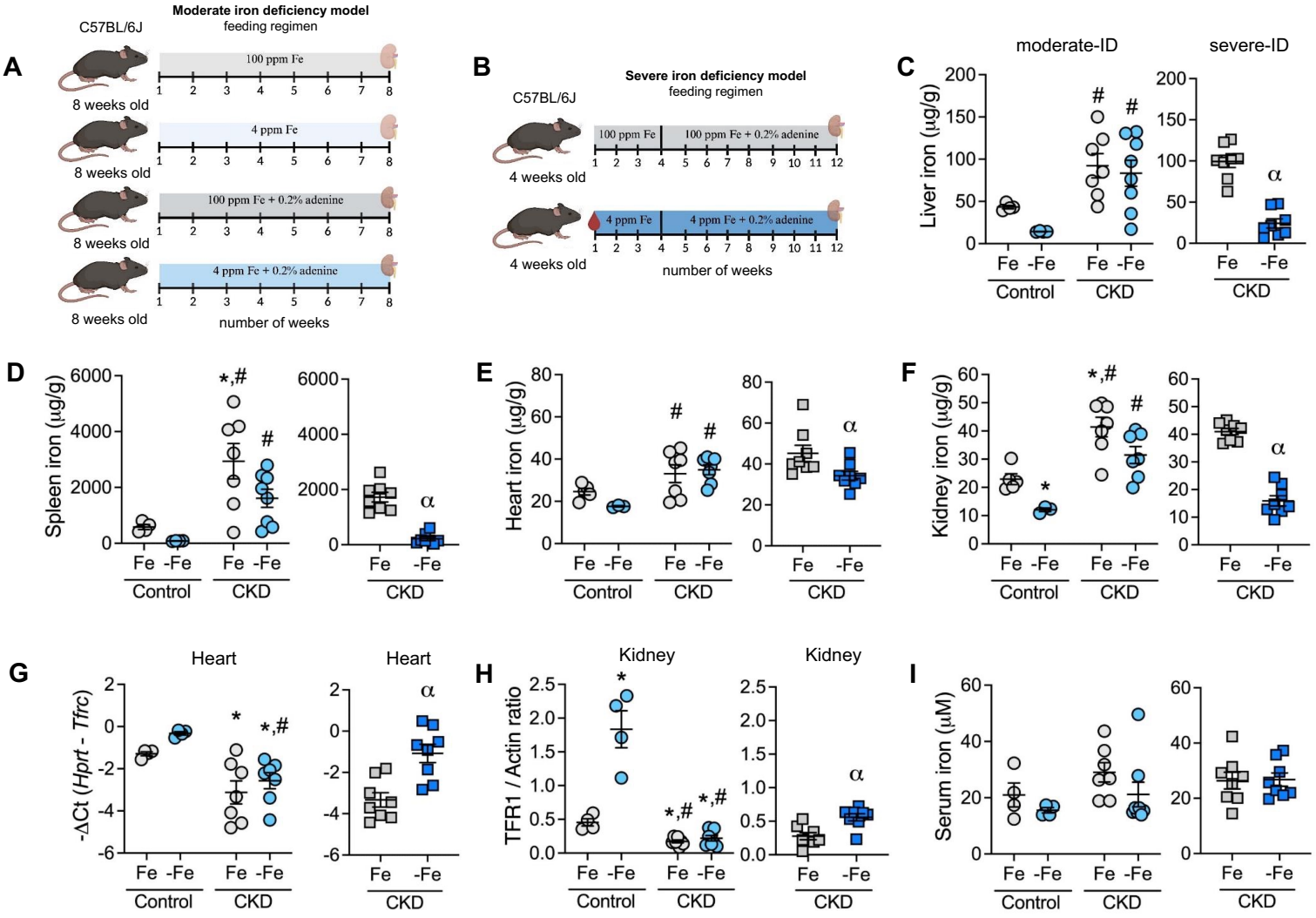
A
Moderate iron deficiency model
feeding regimen
C57BL/6J
100 ppm Fe
8 weeks old
4 ppm Fe
8 weeks old
100 ppm Fe + 0.2% adenine
8 weeks old
4 ppm Fe + 0.2% adenine
8 weeks old
number of weeks
B
Severe iron deficiency model
feeding regimen
C57BL/6J
100 ppm Fe
100 ppm Fe + 0.2% adenine
4 weeks old
4 ppm Fe
4 ppm Fe + 0.2% adenine
4 weeks old
number of weeks
C
moderate-ID
severe-ID
Liver iron (µg/g)
Fe -Fe Fe -Fe
Control CKD
Fe -Fe
CKD
D
Spleen iron (µg/g)
E
Heart iron (µg/g)
F
Kidney iron (µg/g)
G
Heart
-ΔCt (Hprt - Tfrc)
H
Kidney
TFR1 / Actin ratio
I
Serum iron (µM)

Figure 2

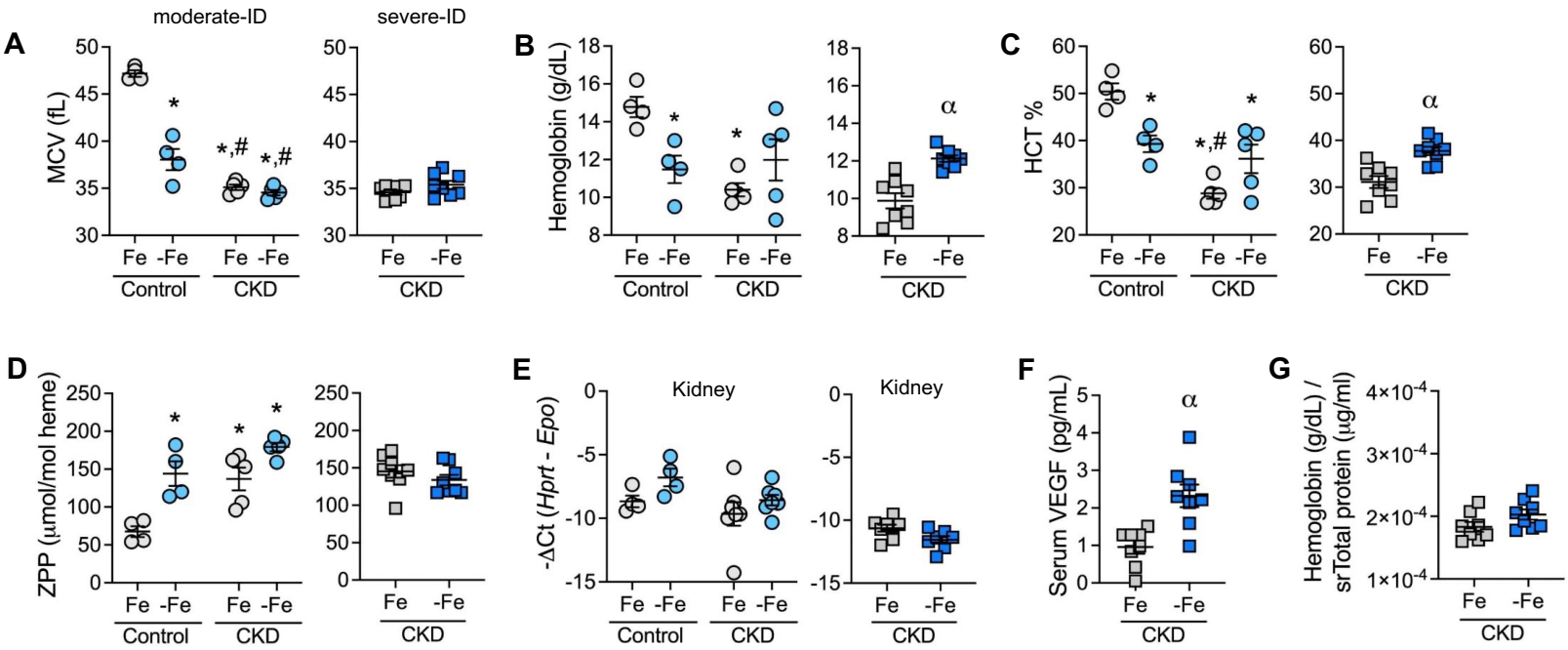
A
moderate-ID
severe-ID
MCV (fL)
Fe -Fe Fe -Fe
Control CKD
Fe -Fe
CKD
B
Hemoglobin (g/dL)
C
HCT %
D
ZPP (µmol/mol heme)
E
-ΔCt (Hprt - Epo)
Kidney
F
Serum VEGF (pg/mL)
G
Hemoglobin (g/dL) / srTotal protein (µg/ml)

Figure 3

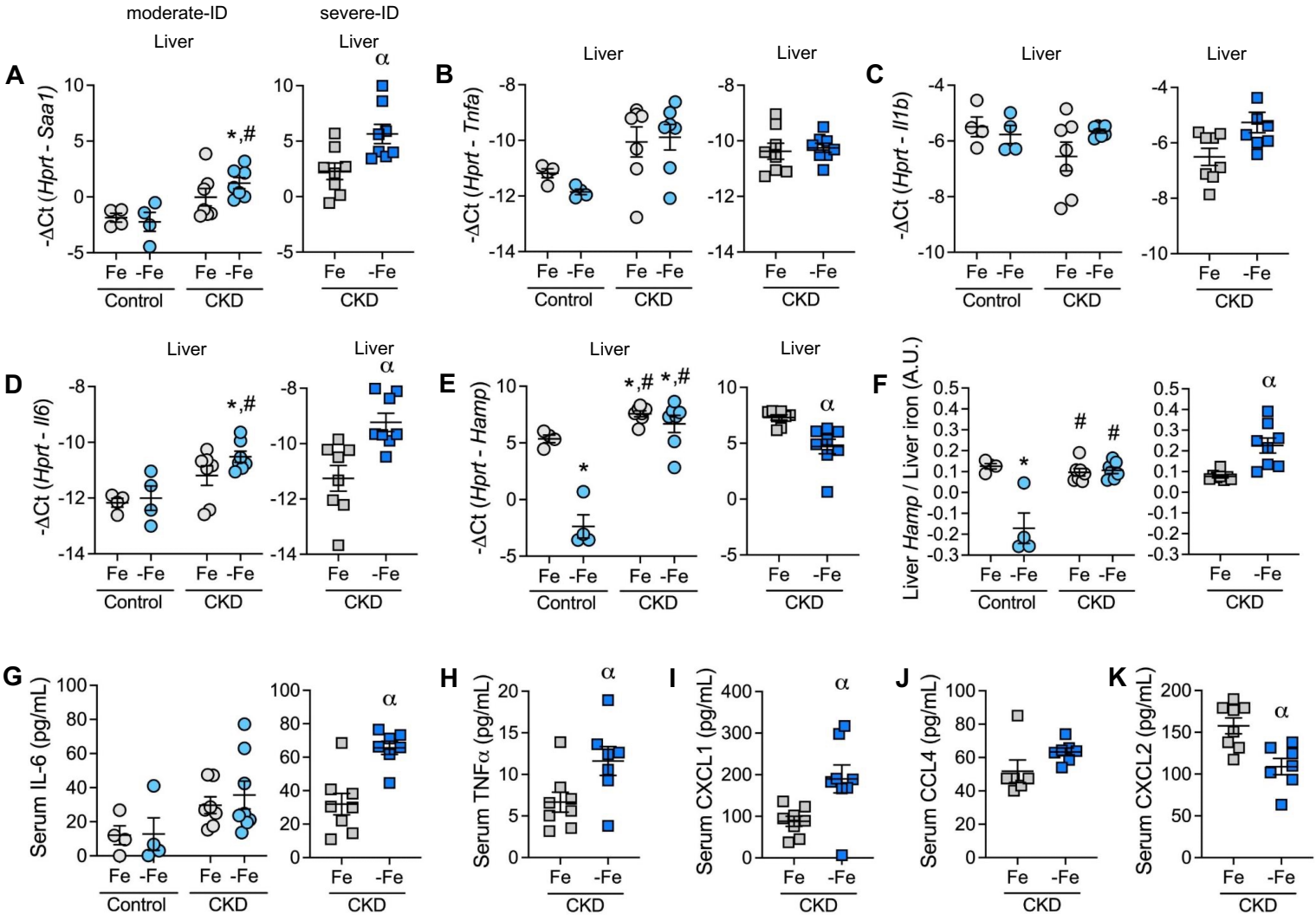
moderate-ID
severe-ID
Liver
A
-ΔCt (Hprt - Saa1)
B
-ΔCt (Hprt - Tnfa)
C
-ΔCt (Hprt - Il1b)
D
-ΔCt (Hprt - Il6)
E
-ΔCt (Hprt - Hamp)
F
Liver Hamp / Liver iron (A.U.)
G
Serum IL-6 (pg/mL)
H
Serum TNFα (pg/mL)
I
Serum CXCL1 (pg/mL)
J
Serum CCL4 (pg/mL)
K
Serum CXCL2 (pg/mL)
Fe
-Fe
Control
CKD
*,#
*
#
α

Figure 4

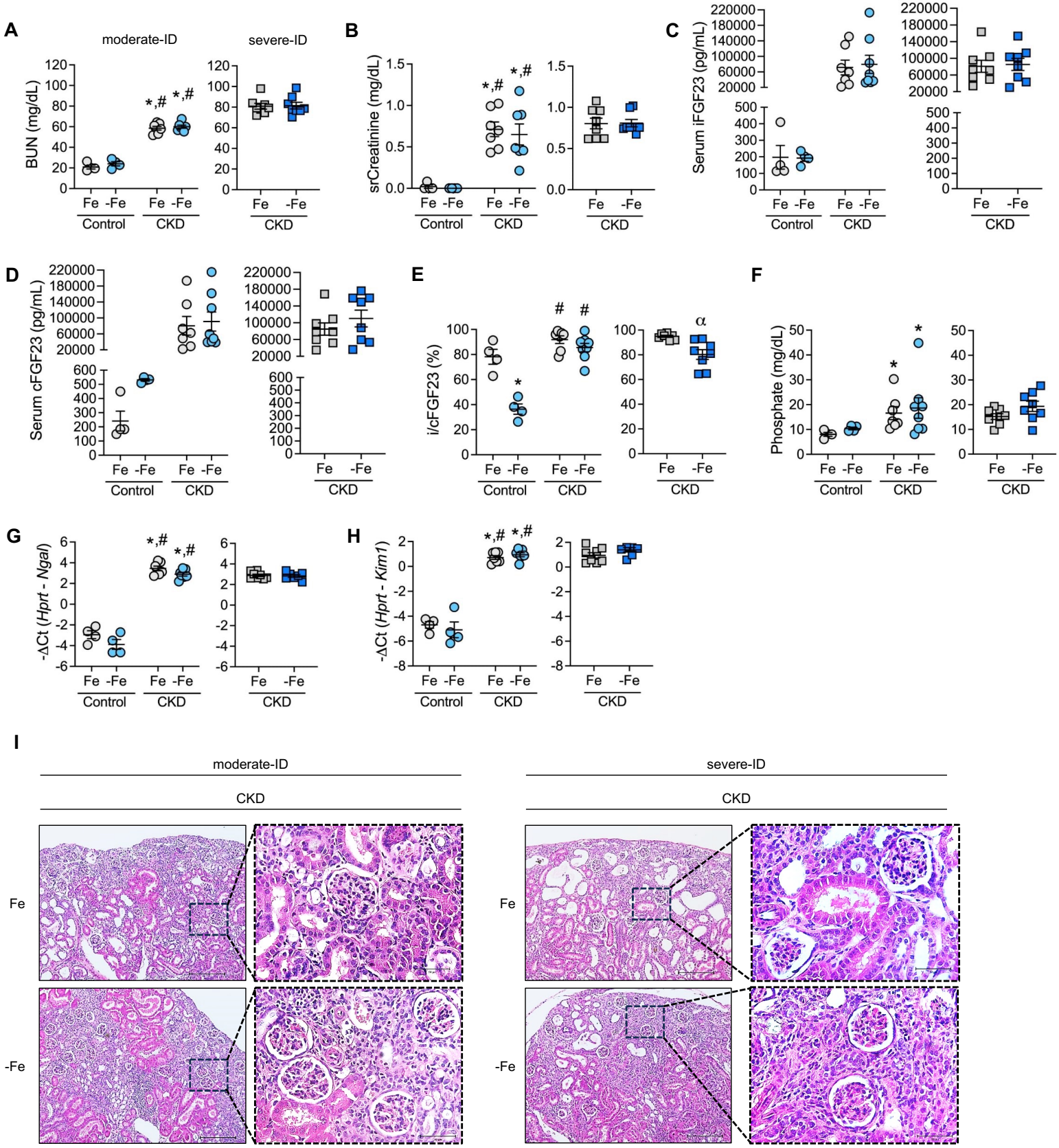
A
moderate-ID
severe-ID
BUN (mg/dL)
B
srCreatinine (mg/dL)
C
Serum iFGF23 (pg/mL)
D
Serum cFGF23 (pg/mL)
E
i/cFGF23 (%)
F
Phosphate (mg/dL)
G
-ΔCt (Hprt - Ngal)
H
-ΔCt (Hprt - Kim1)
Fe
-Fe
Control
CKD
I
moderate-ID
severe-ID
CKD
Fe
-Fe

Figure 5

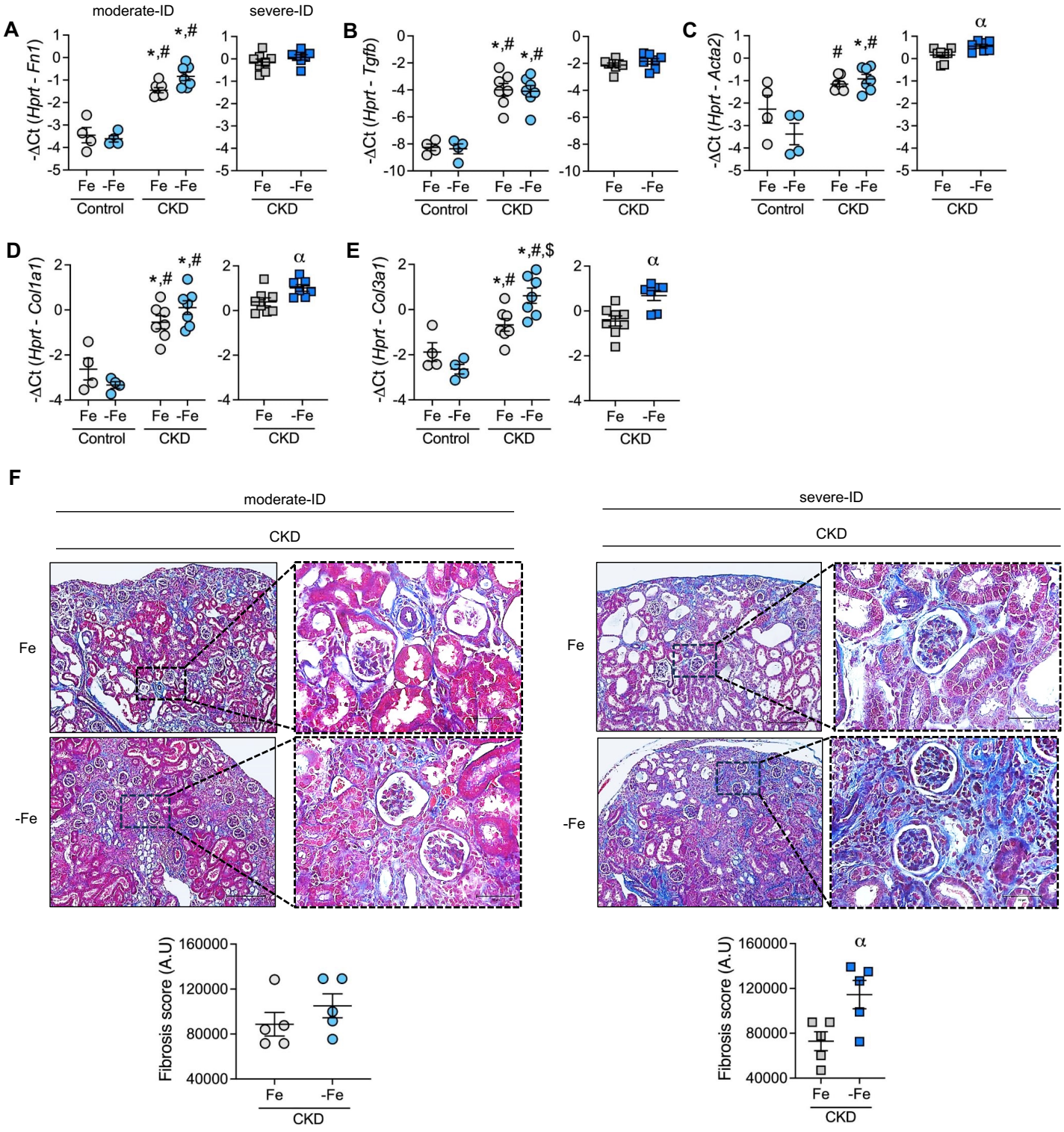
A
moderate-ID
severe-ID
-ΔCt (Hprt - Fn1)
B
-ΔCt (Hprt - Tgfb)
C
-ΔCt (Hprt - Acta2)
D
-ΔCt (Hprt - Col1a1)
E
-ΔCt (Hprt - Col3a1)
Fe
-Fe
Control
CKD
*,#
*,#,$
#
α
F
moderate-ID
severe-ID
CKD
Fe
-Fe
Fibrosis score (A.U)
160000
120000
80000
40000

Figure 6

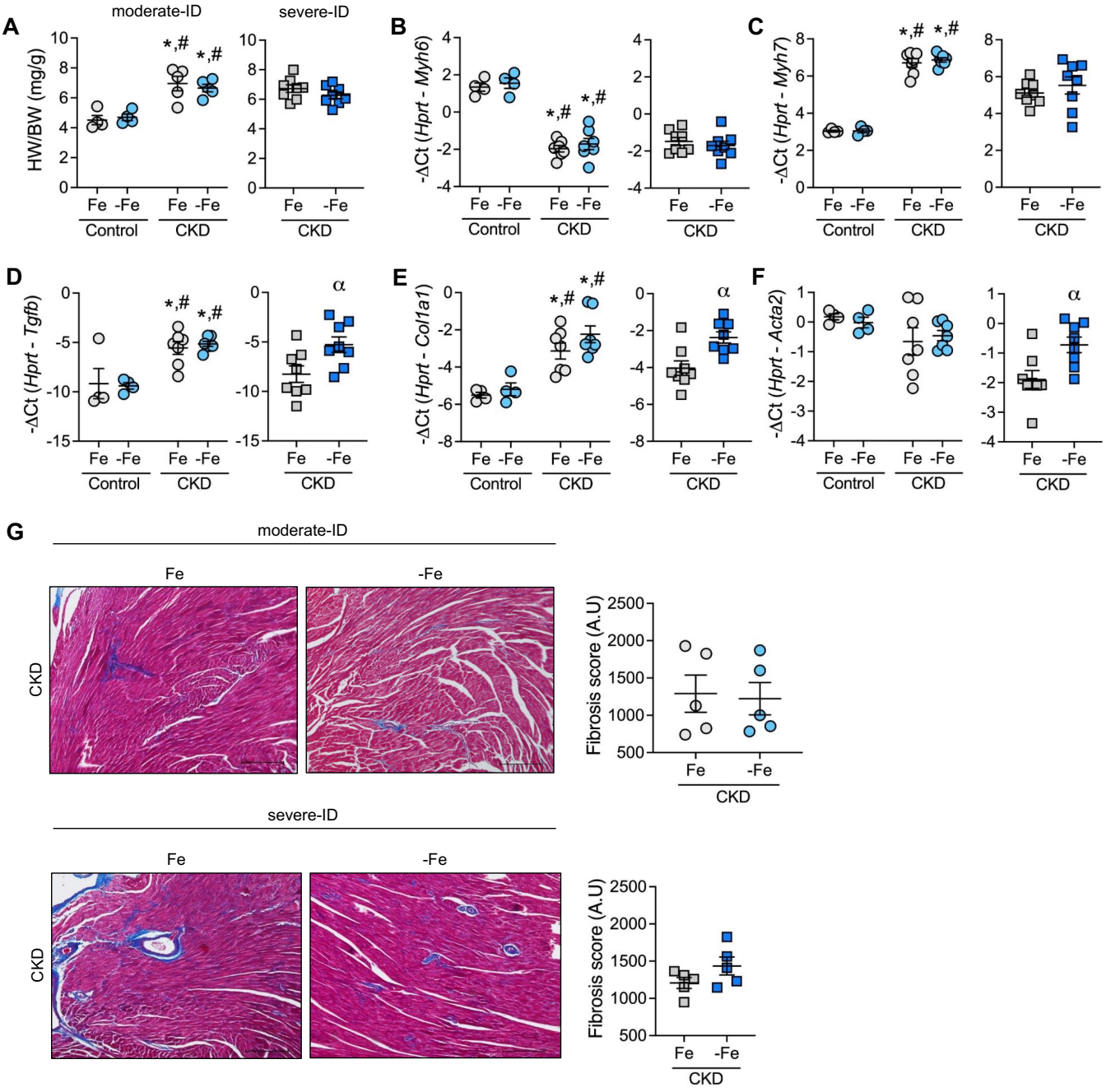
A
moderate-ID
severe-ID
HW/BW (mg/g)
B
-ΔCt (Hprt - Myh6)
C
-ΔCt (Hprt - Myh7)
D
-ΔCt (Hprt - Tgfb)
E
-ΔCt (Hprt - Col1a1)
F
-ΔCt (Hprt - Acta2)
Fe
-Fe
Control
CKD
*,#
α
G
moderate-ID
severe-ID
CKD
Fibrosis score (A.U)

Supplemental Material

Serum chemistry. Serum VEGF levels were assessed by ELISA (UCLA Integrated Molecular Technologies Core). Serum total protein levels were determined by using a Pierce BCA Protein Assay Kit (23227, ThermoFisher Scientific). Serum urea nitrogen (DIUR-100, BioAssay Systems), and serum creatinine (80350, Cayman Chemical) concentrations were measured by colorimetric quantification. Intact FGF23 levels (iFGF23) and C-terminal FGF23 levels (cFGF23; encompassing both intact FGF23 and C-terminal FGF23, serves as a measure of total FGF23) were assessed by ELISA (60-6800, 60-6300, QuidelOrtho). The iFGF23/cFGF23 ratio serves as a proxy indicator of FGF23 cleavage. Serum phosphate levels were assessed by colorimetric quantification (830125, ThermoFisher Scientific). Serum IL-6 levels were measured by ELISA (M6000B, R&D systems). Assays were performed following manufacturers' protocols.

Histology. Kidney and heart tissues were fixed in 10% formalin solution for 24 hours, transferred into 70% ethanol and subjected to paraffin embedding (UCLA Translational Pathology Core Laboratory; TPCL). Kidney and heart sections were cut and either stained with H&E or Masson's trichrome (TPCL) and used for representative images. Images were captured on a Nikon Eclipse E600 microscope with SPOT Basic™ (SPOT Imaging) image capture software. Kidney and heart fibrosis was quantified using ImageJ software.[1-3]

Cytokine and chemokine analysis. Serum cytokine and chemokine concentrations were determined by the UCLA Integrated Molecular Technologies Core using a multiplex bead immunoassay (Millipore Milliplex Cytokine/Chemokine 32-plex Kit on Luminex FlexMap3D), as previously outlined.[4]

Measurement of iron-related and hematologic parameters. Complete blood counts were analyzed by using a HemaVet blood analyzer (Drew Scientific). Zinc protoporphyrin (ZPP) levels were measured using a hematofluorometer (AVIV Biomedical). Serum iron and tissue non-heme iron concentrations were determined by colorimetric quantification per the manufacturer's protocol (157-30, Sekisui Diagnostics). Prior to sampling, liver, spleen, heart, and kidney tissues were pulverized in liquid nitrogen to minimize variation arising from regional differences in tissue iron deposition.

Quantitative PCR. Frozen mouse tissues were pulverized in liquid nitrogen, sampled, and homogenized in TRIzol Reagent (15596018, ThermoFisher Scientific). Total RNA was extracted per manufacturers' protocol. Employing a two-step reaction method, 500 ng of total RNA was reverse transcribed into cDNA using an iScript cDNA Synthesis Kit (1708896, Bio-Rad). Quantitative real-time PCR was performed with 20 ng of cDNA, SsoAdvanced Universal SYBR Green Supermix (172-5272, Bio-Rad) and sequence-specific primers (Supplemental Table 3). Samples were assayed in duplicate with a CFX Connect Real-Time PCR detection system (Bio-Rad). Relative gene expression was normalized to *Hprt* levels. Data are presented as -ΔCt.

Immunoblotting. Kidney tissues were pulverized in liquid nitrogen, sampled, and total protein was extracted through homogenization in RIPA lysis buffer supplemented with protease and phosphatase inhibitors (Sc-24948, Santa Cruz Biotechnology). Lysates were incubated on ice for 30 minutes and cleared by centrifugation at 17,000 g for 30 minutes at 4°C. Supernatants were collected, and protein was quantified using a Pierce BCA Protein Assay Kit (23227, ThermoFisher Scientific).

Protein lysates were prepared in Laemmli-SDS buffer with β-mercaptoethanol as reducing agent (BP-111R, Boston BioProducts), and denatured at 100°C for 5 minutes. Samples were then resolved on Criterion TGX Precast Gels 4-20% (5678094, Bio-Rad), and electroblotted onto nitrocellulose (1704270, Trans-Blot Turbo System, Bio-Rad). Membranes were cut into two parts (100 kDa and 35 kDa) and were blocked and probed with either mouse monoclonal antibody against transferrin receptor 1 at 1:10,000 (TFR1; 13-6800, Invitrogen) or mouse monoclonal antibody against β-actin-peroxidase at 1:30,000 (A3854, Sigma-Aldrich), and incubated overnight at 4°C. Next day, membranes were washed, and either directly imaged with a ChemiDoc XRS+ system (Bio-Rad) to visualize β-actin, or probed with anti-mouse IgG HRP (367076s, Cell Signaling) at 1:3,000 for 1 hour at room temperature, and imaged to visualize TFR1. Quantitation with normalization to β-actin was performed using Image Lab Software, version 5.2.1 (Bio-Rad).

Statistical analysis. Data organization, scientific graphing, and statistical significance of differences between experimental groups were performed by using GraphPad Prism (version 10.2.3). Data are presented as individual values, with mean ± SEM. Statistical differences between groups were either determined by a two-way analysis of variance (ANOVA) followed by a post hoc Tukey test, or by an unpaired-*t*-test with Welch's correction (two-tailed). Statistical test, number of animals per group, and *P*-value are indicated in each figure panel and legend. A *P*-value of <0.05 was considered significant.

Supplemental References

1. Haub, P., and Meckel, T. (2015). A Model based Survey of Colour Deconvolution in Diagnostic Brightfield Microscopy: Error Estimation and Spectral Consideration. Sci Rep *5*, 12096. 10.1038/srep12096.
2. Landini, G., Martinelli, G., and Piccinini, F. (2021). Colour deconvolution: stain unmixing in histological imaging. Bioinformatics *37*, 1485-1487. 10.1093/bioinformatics/btaa847.
3. Ruifrok, A.C., and Johnston, D.A. (2001). Quantification of histochemical staining by color deconvolution. Anal Quant Cytol Histol *23*, 291-299.
4. Fisher, A.L., Sangkhae, V., Balusikova, K., Palaskas, N.J., Ganz, T., and Nemeth, E. (2021). Iron-dependent apoptosis causes embryotoxicity in inflamed and obese pregnancy. Nat Commun *12*, 4026. 10.1038/s41467-021-24333-z.

Supplemental Table 1. Macroscopic parameters of iron-replete and moderate-ID mice receiving control or adenine diet.

	Fe + control	-Fe + control	Fe + CKD	-Fe + CKD
Body weight (g)	27.5 ± 1.6	26.2 ± 1.1	18.4*# ± 1.7	21.1 ± 2.1
Liver weight (g)	1.23 ± 0.1	1.03 ± 0.03	0.89* ± 0.7	0.82* ± 0.04
Spleen weight (mg)	73.3 ± 2.1	92.8* ± 2.8	59.2*# ± 5.2	79.4*#$ ± 3.3
Heart weight (mg)	123.0 ± 5.1	122.5 ± 5.1	125.0 ± 3.8	138.8 ± 9.7
Kidney weight (mg)	318.8 ± 9.9	299.8 ± 4.8	238.4*# ± 5.5	233.2*# ± 3.1

Moderate-ID model in mice fed iron-replete (100ppm; Fe) or iron-deficient (4ppm; -Fe) diets, with or without 0.2% adenine to induce CKD. Values are mean ± SEM. Comparison between groups analyzed by two-way ANOVA with Tukey post hoc test. N=4-5/group; *$p \leq 0.05$ vs. Fe+ control diet, #$p \leq 0.05$ vs. -Fe + control, \$$p \leq 0.05$ vs. Fe + CKD. Kidney weight represents combined weights of left and right kidney.

Supplemental Table 2. Macroscopic parameters of iron-replete and severe-ID mice receiving adenine diet.

	Fe + CKD	-Fe + CKD
Body weight (g)	17.2 ± 0.5	21.2* ± 1.3
Liver weight (g)	1.05 ± 0.08	0.99 ± 0.06
Spleen weight (mg)	54.3 ± 5.7	84.4* ± 9.4
Heart weight (mg)	115.0 ± 4.9	132.2 ± 7.2
Kidney weight (mg)	239.1 ± 4.2	246.6 ± 3.1

Severe-ID model in mice fed iron-replete (100ppm; Fe) or iron-deficient (4ppm; -Fe) diets containing 0.2% adenine to induce CKD. Values are mean ± SEM. Comparison between groups analyzed by unpaired-*t*-test with Welch's correction (two-tailed). N=8/group; *$p \leq 0.05$ vs. Fe + CKD. Kidney weight represents combined weights of left and right kidney.

Supplemental Table 3. Oligonucleotides used as sequence specific primers in qPCR.

Gene	Species	Orientation	Primer Sequence (5' – 3')
Acta2	Mus musculus	Forward Reverse	GTC CCA GAC ATC AGG GAG TAA TCG GAT ACT ACT TCA GCG TCA GGA
Col1a1	Mus musculus	Forward Reverse	ATG GAT TCC CGT TCG AGT ACG TCA GCT GGA TAG CGA CAT CG
Col3a1	Mus musculus	Forward Reverse	GAC CAA AAG GTG ATG CTG GAC AG CAA GAC CTC GTG CTC CAG TTA G
Ctgf/Ccn2	Mus musculus	Forward Reverse	TGC GAA GCT GAC CTG GAG GAA A CCG CAG AAC TTA GCC CTG TAT G
Fn1	Mus musculus	Forward Reverse	GAT GTC CGA ACA GCT ATT TAC CA CCT TGC GAC TTC AGC CAC T
Hamp	Mus musculus	Forward Reverse	GAG CAG CAC CAC CTA TCT CC TTG GTA TCG CAA TGT CTG CC
Hprt	Mus musculus	Forward Reverse	CTG GTT AAG CAG TAC AGC CCC AA CGA GAG GTC CTT TTC ACC AGC
Il1b	Mus musculus	Forward Reverse	TGC CAC CTT TTG ACA GTG ATG TGA TGT GCT GCT GCG AGA TT
Il6	Mus musculus	Forward Reverse	CTC TGG GAA ATC GTG GAA AT CCA GTT TGG TAG CAT CCA TC
Kim1/Havcr1	Mus musculus	Forward Reverse	CGA GTG GAG ATT CCT GGA TGG GGA CGT GTG GGA ATC TCT GG
Myh6	Mus musculus	Forward Reverse	GCC CAG TAC CTC CGA AAG TC ATC AGG CAC GAA GCA CTC C
Myh7	Mus musculus	Forward Reverse	GCT GGA AGA TGA GTG CTC AGA G TCC AAA CCA GCC ATC TCC TCT G
Ngal/Lcn2	Mus musculus	Forward Reverse	GTC CCC ACC GAC CAA TGC ATT GGG TCT CTG CGC ATC C
Opn/Spp1	Mus musculus	Forward Reverse	AGC AAG AAA CTC TTC CAA GCA A GTG AGA TTC GTC AGA TTC ATC CG
Runx2	Mus musculus	Forward Reverse	GAC TGT GGT TAC CGT CAT GGC ACT TGG TTT TTC ATA ACA GCG GA
Saa1	Mus musculus	Forward Reverse	ACA CCA GCA GGA TGA AGC TAC T GAG CAT GGA AGT ATT TGT CTG AGT
Sox9	Mus musculus	Forward Reverse	CAG CCC CTT CAA CCT TCC TC TGA TGG TCA GCG TAG TCG TAT T
Tgfb	Mus musculus	Forward Reverse	ATA CGT CAG ACA TTC GGG AAG CAG TG AAT AGT TGG TAT CCA GGG CTC TCC G
Tfrc	Mus musculus	Forward Reverse	TCA TGA GGG AAA TCA ATG AT GCC CCA GAA GAT ATG TCG GAA
Tnfa	Mus musculus	Forward Reverse	CCC TCA CAC TCA GAT CAT CTT CT GCT ACG ACG TGG GCT ACAG

Epo	Mus musculus	Forward Reverse	TCT ACG TAG CCT CAC TTC ACT ACC CGG AAG AGC TTG CAG AAA

Supplemental Figure 1

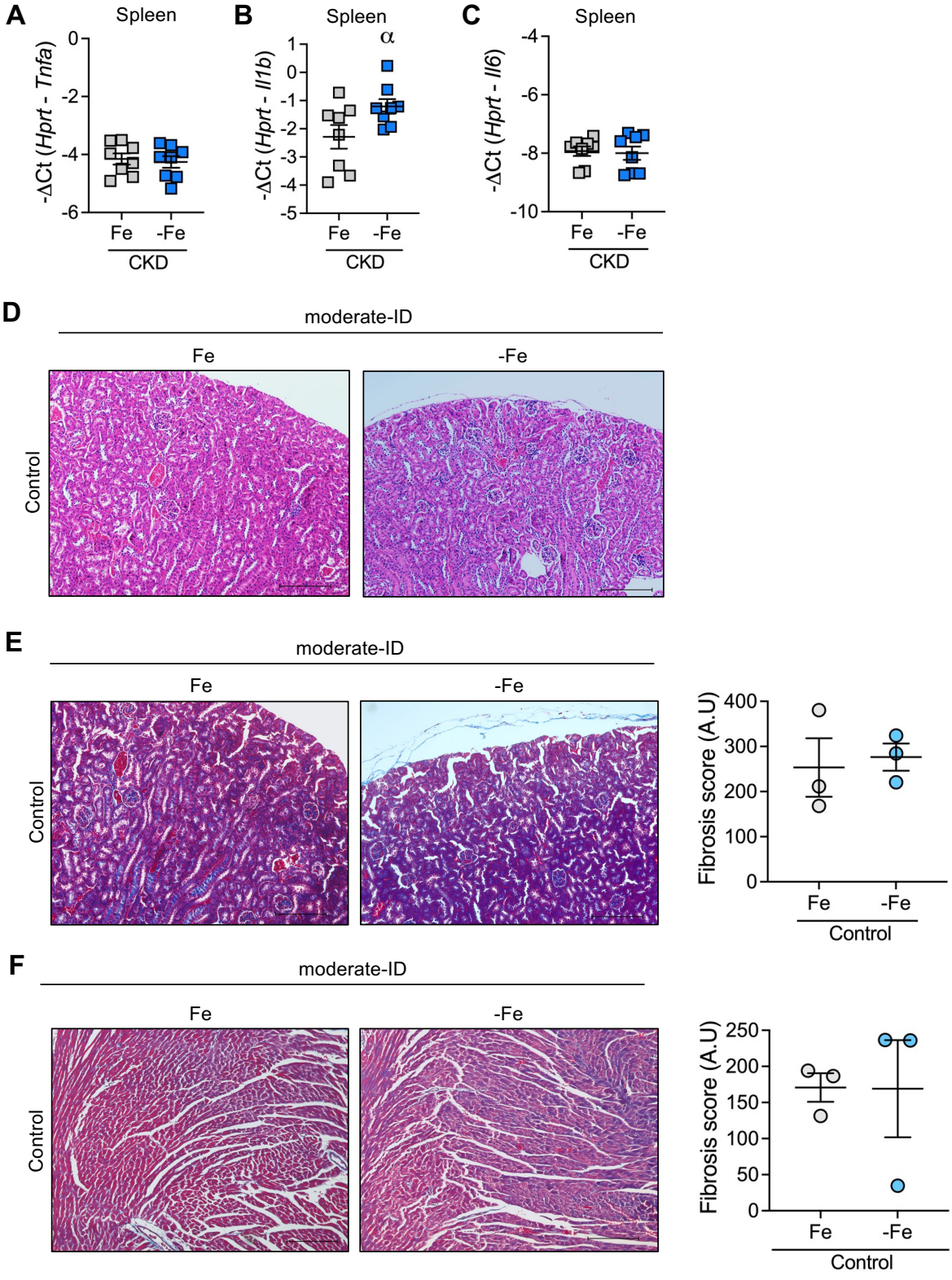

Supplemental Figure 1. Severe-ID in adenine-induced CKD augments splenic *Il1b* expression and histological assessment of non-CKD controls.

Moderate and severe-ID models in mice fed iron-replete (100 ppm; Fe) or iron-deficient (4 ppm; -Fe) diets, with or without 0.2% adenine to induce CKD. Quantitative PCR (qPCR) analysis of *Tnfa* (**A**), *Il1b* (**B**), *Il6* (**C**) expression in spleen tissue of severe-ID model. Representative H&E-stained kidney (**D**), and Masson's trichrome-stained kidney (**E**) and heart (**F**) sections of moderate-ID model controls with quantification shown as fibrosis score; n=3 mice/group (original magnification, 10x; scale bar, 200 um). Data are mean ± SEM (n = 8 mice/group; $^{\alpha}p \leq 0.05$ vs. replete + adenine diet) analyzed by unpaired-*t*-test with Welch's correction (two-tailed) for severe-ID.

Supplemental Figure 2

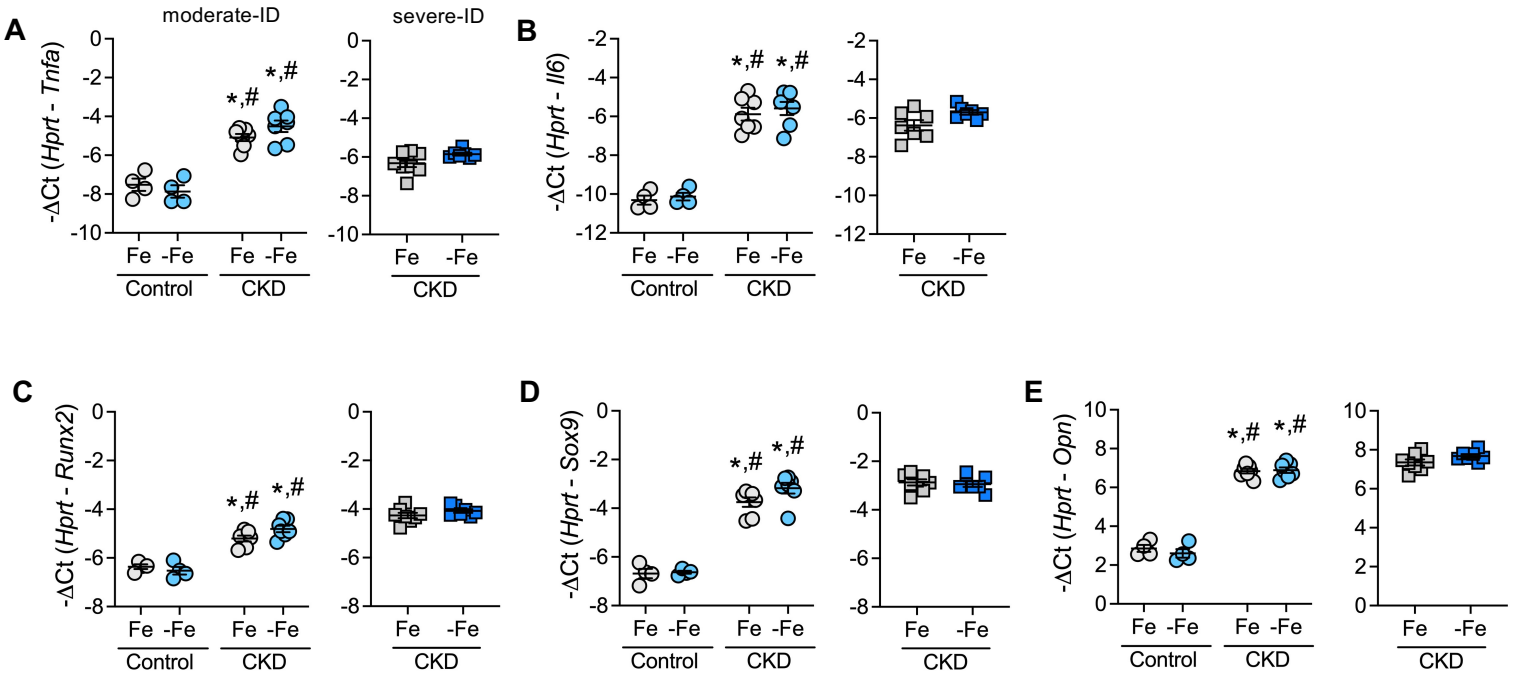

Supplemental Figure 2. Iron deficiency does not exacerbate kidney inflammation or calcification in adenine-induced CKD.

Moderate and severe-ID models in mice fed iron-replete (100 ppm; Fe) or iron-deficient (4 ppm; -Fe) diets, with or without 0.2% adenine to induce CKD. qPCR analysis of *Tnfa* (**A**), *Il6* (**B**), *Runx2* (**C**), *Sox9* (**D**) and *Opn* (**E**) expression in kidney tissue. Data are mean ± SEM (n = 4–7 mice/group; *p ≤ 0.05 vs. Fe + control, #p ≤ 0.05 vs. -Fe + control; n = 7-8 mice/group; no statistical significance) analyzed by two-way ANOVA with Tukey post hoc test for moderate-ID, or unpaired-*t*-test with Welch's correction (two-tailed) for severe-ID.

Supplemental Figure 3

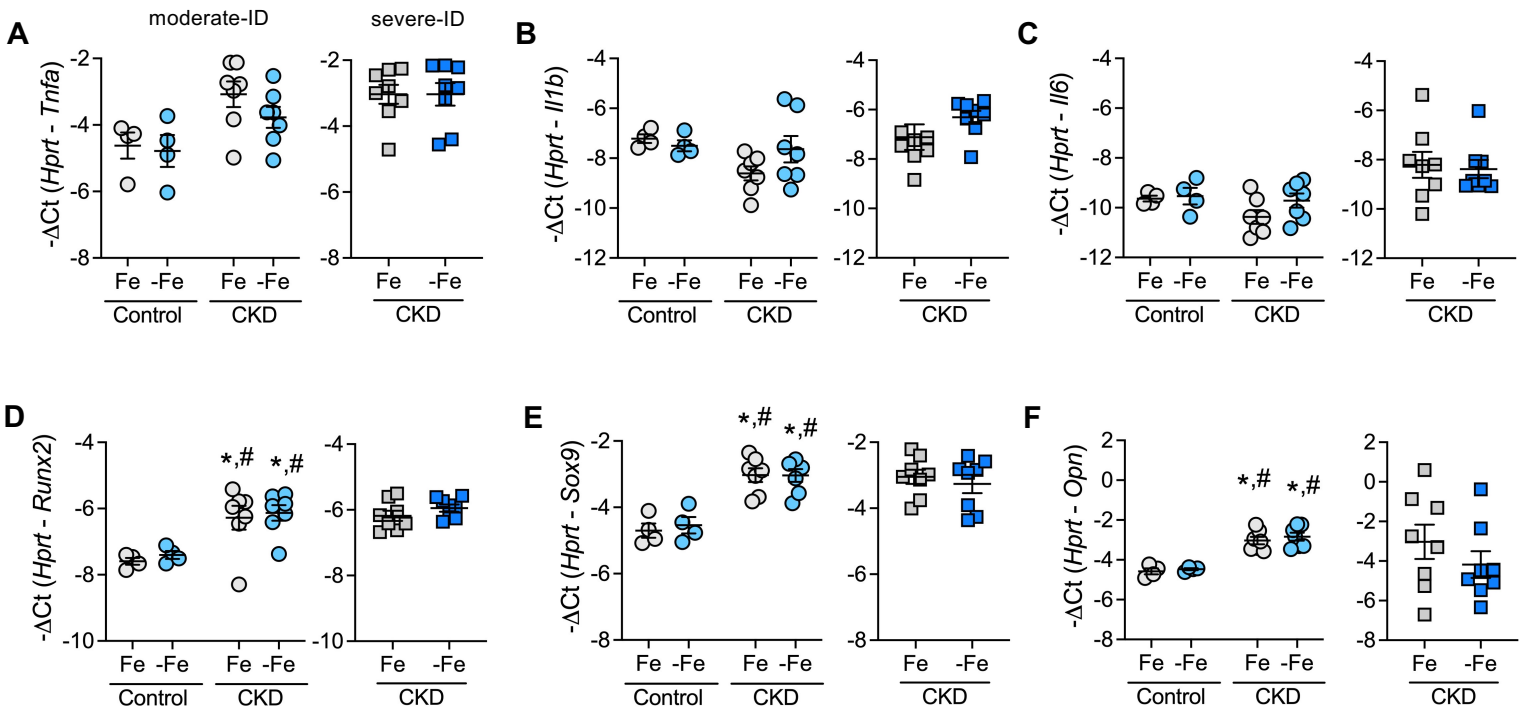

Supplemental Figure 3. Iron deficiency does not exacerbate cardiac inflammation or calcification in adenine-induced CKD.

Moderate and severe-ID models in mice fed iron-replete (100 ppm; Fe) or iron-deficient (4 ppm; -Fe) diets, with or without 0.2% adenine to induce CKD. qPCR analysis of *Tnfa* (**A**), *Il1b* (**B**), *Il6* (**C**), *Runx2* (**D**), *Sox9* (**E**) and *Opn* (**F**) expression in heart tissue. Data are mean ± SEM (n = 4–7 mice/group; *p ≤ 0.05 vs. Fe + control, #p ≤ 0.05 vs. -Fe + control; n = 8 mice/group; no statistical significance) analyzed by two-way ANOVA with Tukey post hoc test for moderate-ID, or unpaired-*t*-test with Welch's correction (two-tailed) for severe-ID.

Supplemental Figure 4

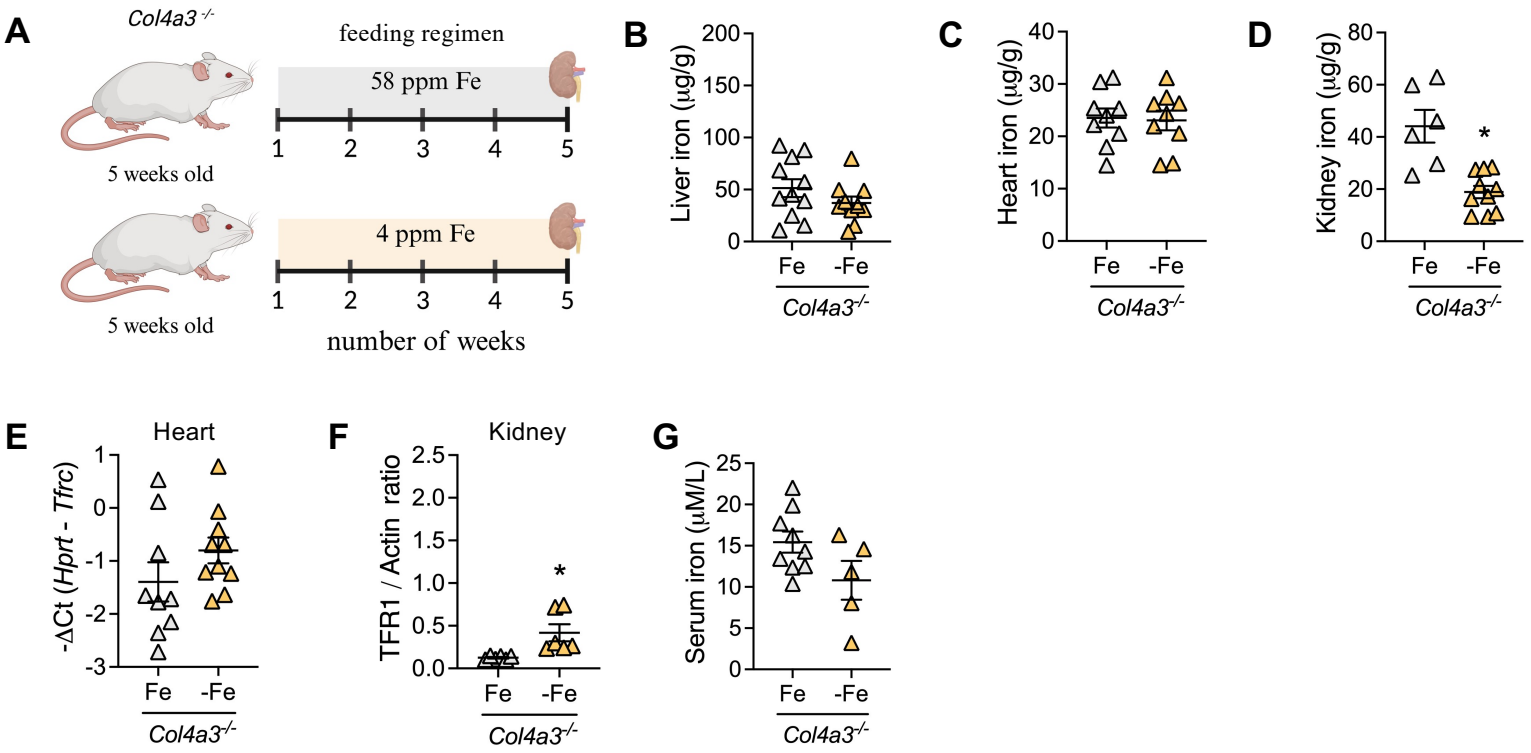

Supplemental Figure 4. Establishment of graded iron-deficiency in *Col4a3*$^{-/-}$ (Alport syndrome) mice.

(**A**) Schematic of moderate-iron deficiency (ID) model in *Col4a3*$^{-/-}$ mice fed iron-replete (58 ppm; Fe) or iron-deficient (4 ppm; -Fe) diets. Non-heme iron levels in liver (**B**), heart (**C**) and kidney (**D**) tissue. qPCR analysis of *Tfrc* (**E**) expression in heart tissue. (**F**) Densitometry TFR1 protein levels in kidney tissue. (**G**) Serum iron levels. Data are mean ± SEM (n = 5–11 mice/group; *p ≤ 0.05 vs. Fe + *Col4a3*$^{-/-}$) analyzed by unpaired-*t*-test with Welch's correction (two-tailed).

Supplemental Figure 5

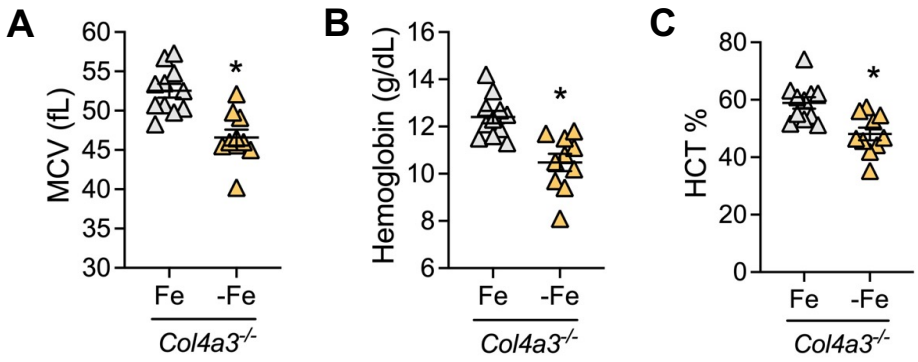

Supplemental Figure 5. Effects of graded iron deficiency on complete blood count parameters in *Col4a3*$^{-/-}$ (Alport syndrome) mice.

Moderate-ID model in *Col4a3*$^{-/-}$ mice fed iron-replete (58 ppm; Fe) or iron-deficient (4 ppm; -Fe) diets. Measured parameters include (**A**) mean corpuscular volume (MCV), (**B**) hemoglobin, (**C**) hematocrit percentage (HCT%). Data are mean ± SEM (n = 9–11 mice/group; *$p \leq 0.05$ vs. Fe + *Col4a3*$^{-/-}$) analyzed by unpaired-*t*-test with Welch's correction (two-tailed).

Supplemental Figure 6

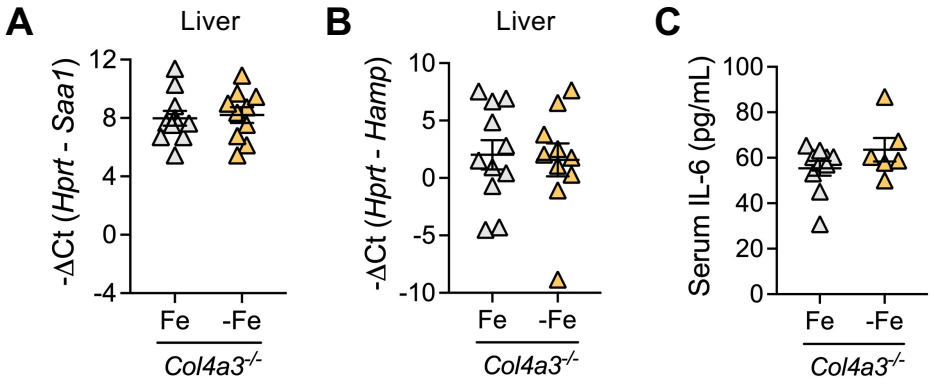

Supplemental Figure 6. Iron deficiency does not alter systemic inflammation or hepatic *Hamp* expression in *Col4a3*$^{-/-}$ (Alport syndrome) mice.

Moderate-ID model in *Col4a3*$^{-/-}$ mice fed iron-replete (58 ppm; Fe) or iron-deficient (4 ppm; -Fe) diets. qPCR analysis of *Saa1* (**A**) and *Hamp* (**B**) expression in liver tissue. (**C**) Serum IL-6 levels. Data are mean ± SEM (n = 6–11 mice/group; no statistical significance) analyzed by unpaired-*t*-test with Welch's correction (two-tailed).

Supplemental Figure 7

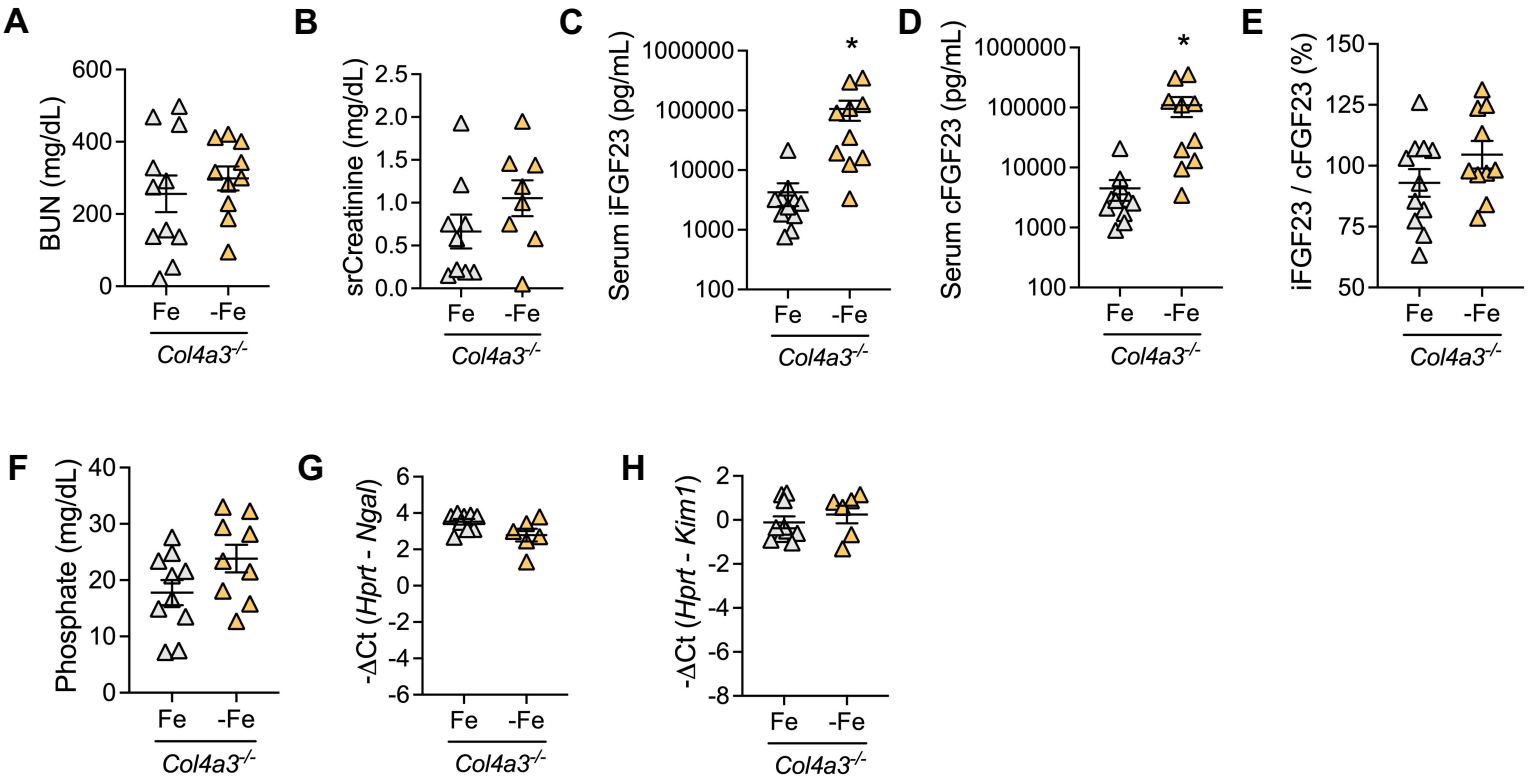

Supplemental Figure 7. Iron deficiency does not aggravate renal injury or dysfunction in *Col4a3*$^{-/-}$ (Alport syndrome) mice.

Moderate-ID model in *Col4a3*$^{-/-}$ mice fed iron-replete (58 ppm; Fe) or iron-deficient (4 ppm; -Fe) diets. Measured parameters include (**A**) blood urea nitrogen (BUN), (**B**) serum creatinine, (**C**) serum intact FGF23, (**D**) serum c-terminal FGF23, (**E**) intact FGF23 relative to c-terminal FGF23, (**F**) serum phosphate. qPCR analysis of *Ngal* (**G**) and *Kim1* (**H**) expression in kidney tissue. Data are mean ± SEM (n = 6–11 mice/group; *p ≤ 0.05 vs. Fe + *Col4a3*$^{-/-}$) analyzed by unpaired-*t*-test with Welch's correction (two-tailed).

Supplemental Figure 8

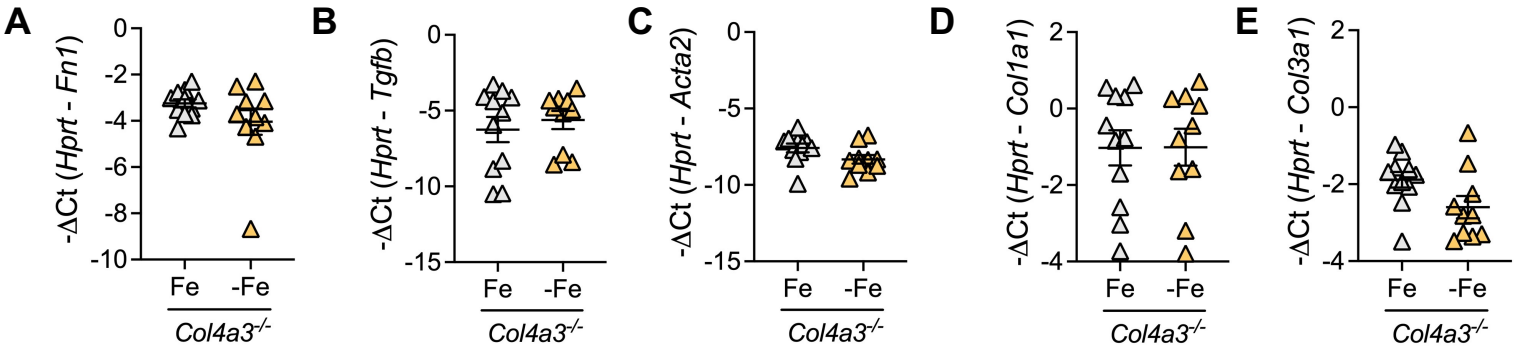

Supplemental Figure 8. Iron deficiency does not aggravate renal fibrosis in *Col4a3*$^{-/-}$ (Alport syndrome) mice.

Moderate-ID model in *Col4a3*$^{-/-}$ mice fed iron-replete (58 ppm; Fe) or iron-deficient (4 ppm; -Fe) diets. qPCR analysis of *Fn1* (**A**), *Tgfb* (**B**), *Acta2* (**C**), *Col1a1* (**D**) and *Col3a1* (**E**) expression in kidney tissue. Data are mean ± SEM (n = 10–11 mice/group; no statistical significance) analyzed by unpaired-*t*-test with Welch's correction (two-tailed).

Supplemental Figure 9

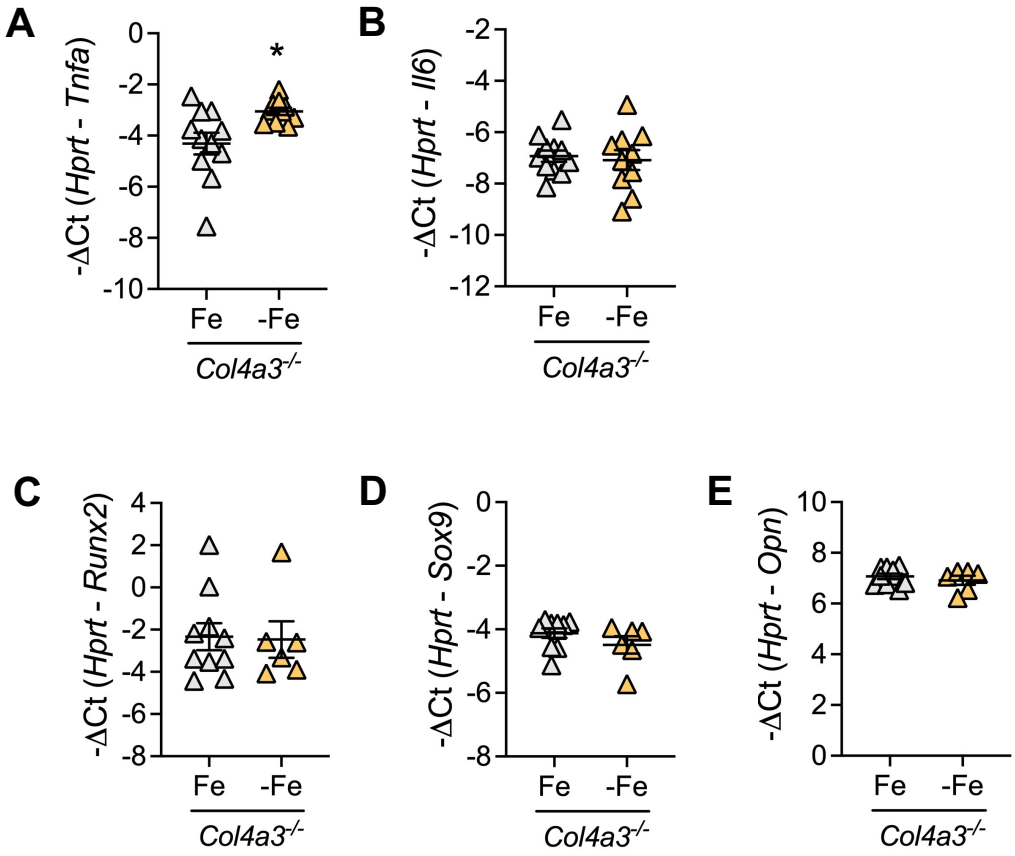

Supplemental Figure 9. Graded iron deficiency increases renal *Tnfa* mRNA expression but does not aggravate renal calcification in *Col4a3*$^{-/-}$ (Alport syndrome) mice.

Moderate-ID model in *Col4a3*$^{-/-}$ mice fed iron-replete (58 ppm; Fe) or iron-deficient (4 ppm; -Fe) diets. qPCR analysis of *Tnfa* (**A**), *Il6* (**B**), *Runx2* (**C**), *Sox9* (**D**) and *Opn* (**E**) expression in kidney tissue. Data are mean ± SEM (n = 6–11 mice/group; *p ≤ 0.05 vs. Fe + *Col4a3*$^{-/-}$) analyzed by unpaired-*t*-test with Welch's correction (two-tailed).

Supplemental Figure 10

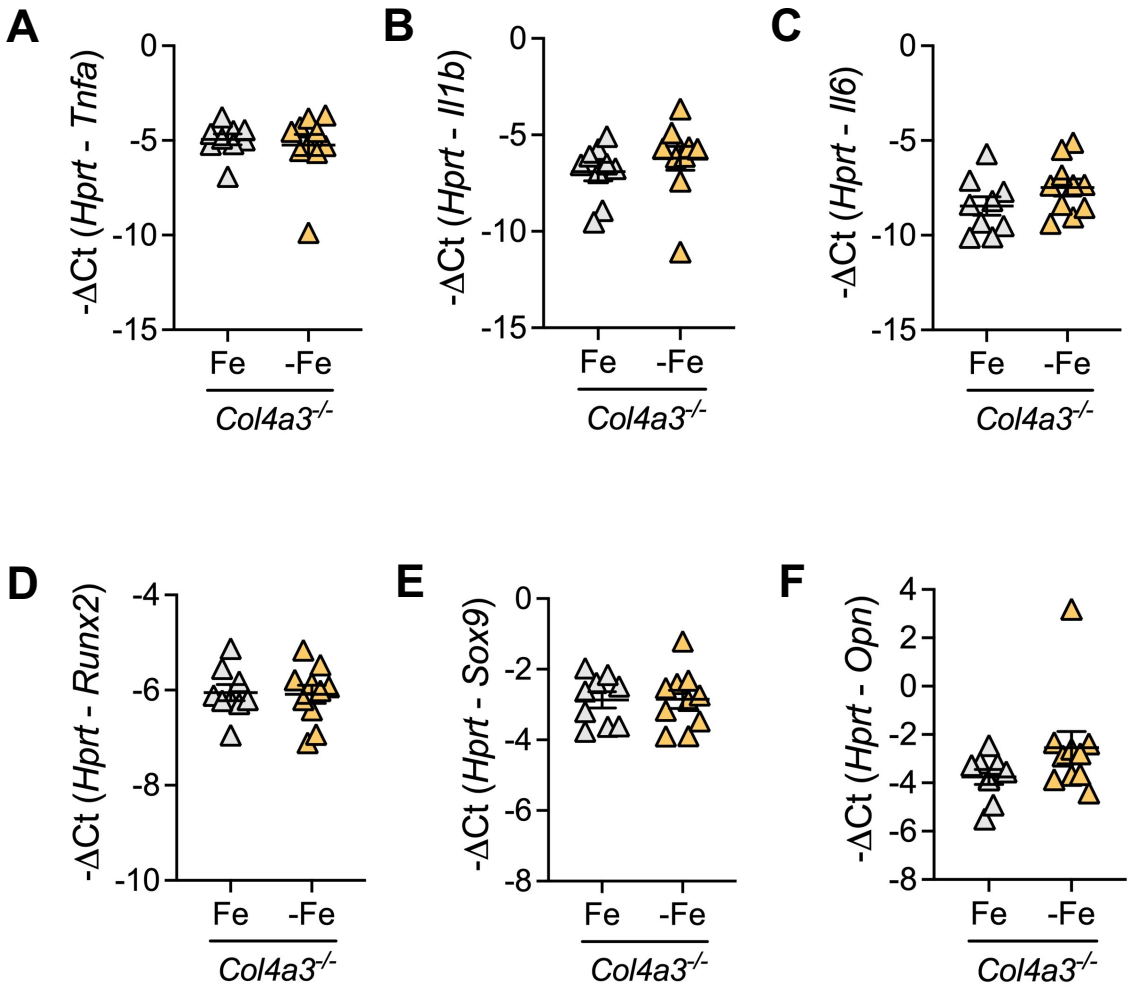

Supplemental Figure 10. Iron deficiency does not aggravate cardiac inflammation or calcification in *Col4a3*$^{-/-}$ (Alport syndrome) mice.

Moderate-ID model in *Col4a3*$^{-/-}$ mice fed iron-replete (58 ppm; Fe) or iron-deficient (4 ppm; -Fe) diets. qPCR analysis of *Tnfa* (**A**), *Il1b* (**B**), *Il6* (**C**), *Runx2* (**D**), *Sox9* (**E**) and *Opn* (**F**) expression in heart tissue. Data are mean ± SEM (n = 9–11 mice/group; no statistical significance) analyzed by unpaired-*t*-test with Welch's correction (two-tailed).

Supplemental Figure 11

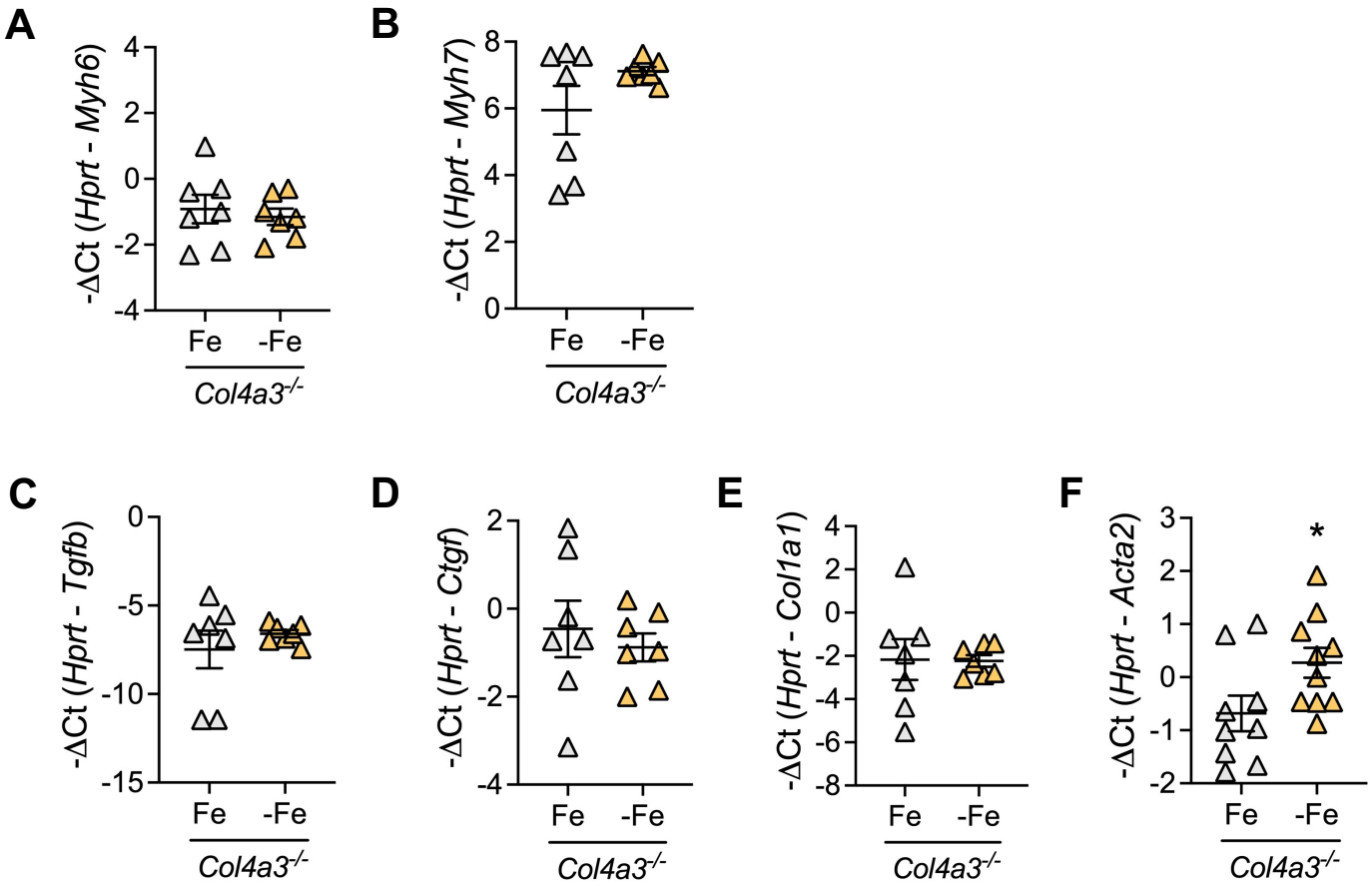

Supplemental Figure 11. Graded iron deficiency augments cardiac *Acta2* mRNA expression but does not aggravate cardiac injury or overall fibrosis in *Col4a3*$^{-/-}$ (Alport syndrome) mice.

Moderate-ID model in *Col4a3*$^{-/-}$ mice fed iron-replete (58 ppm; Fe) or iron-deficient (4 ppm; -Fe) diets. qPCR analysis of *Myh6* (**A**), *Myh7* (**B**), *Tgfb* (**C**), *Ctgf* (**D**), *Col1a1* (**E**) and *Acta2* (**F**) expression in heart tissue. Data are mean ± SEM (n = 7 mice/group; *p ≤ 0.05 vs. Fe + *Col4a3*$^{-/-}$) analyzed by unpaired-*t*-test with Welch's correction (two-tailed).